UNIVERSITY OF CALIFORNIA

Santa Barbara

Reconstructing Fire Severity and Post-Fire Recovery in a Southern California Watershed Using Hyperspectral Imagery and LiDAR

A Thesis submitted in partial satisfaction of the

requirements for the degree Master of Arts

in Geography

by

Mingquan Chen

Committee in charge:

Professor Dar Roberts, Chair

Professor Keith Clarke

Professor Stuart Sweeney

March 2017

The thesis of Mingquan Chen is approved.

_____

Stuart Sweeney

_____

Keith Clarke

_____

Dar Roberts, Committee Chair

March 2017

Reconstructing Fire Severity and Post-Fire Recovery in a Southern California Watershed Using Hyperspectral Imagery and LiDAR

by

Mingquan Chen

ACKNOWLEDGEMENTS

My work on this thesis would not be possible without the generous support of many colleagues, friends, and family.

First, I would like to thank my advisor, Professor Dar Roberts for offering me the opportunity to study at UCSB and keeping a door open whenever I ran into troubles or questions. Not only has Dar taught me how to conduct science and teaching, but also the way of scientific thinking. I was also lucky to have Professor Keith Clarke and Professor Stuart Sweeney on my committee. Keith's general interests in GIScience helps me complete the story of my thesis, while Stuart brings me back to key issues of statistical analysis after running all those remote sensing images.

This work was supported by the US National Science Foundation's Long Term Ecological Research program and OCE-9982105, OCE-0620276, OCE-1232779. I acknowledge the Santa Barbara Coastal Long Term Ecological Research Project (SBC) to make it happen. Special thanks to John Potapenko, Erin Wetherley and Professor Bodo Bookhagen for helping me get started with related data processing.

Thanks to all VIPER Lab members for providing support on my study, and more importantly, for helping me get used to American life and culture. I owe a shout-out to Susan Meerdink for being a great graduate cohort, who always seems to enjoy helping with my questions as much as working on her own. I owe special thanks to Seth Peterson for preprocessing various

remote sensing data, also his delicious homemade yogurt which proves that not all Asians are allergic to milk!

Thanks to all my Chinese cohort/friends in Geography Department/UCSB, for cheering me up when I feel homesick. Their names are too many to list, but among them are Song Gao, Runsheng Song, Honglei Liu, Rui Wu, Junkai Jiang, Zhen Bi, Yiting Ju, Yingjie Hu, Yang Lin, Jie Dai, Xiaoli Chen, Yu Yu, Chong Huang, Xin Feng, Rui Zhu, Haiyun Ye, Bo Yan and Qi He.

Finally, I want to dedicate this dissertation to my parents, Dahong and Xiaoyu, who deserves infinite credit for the support throughout the years of my life and education. They have supported me spiritually, intellectually, and financially.

The way that can be told is not the eternal way.

The name that can be named is not the eternal name.

Lao Tzu – 'Tao Te Ching'
老子 –《道德经》

ABSTRACT

Reconstructing Fire Severity and Post-Fire Recovery in a Southern California Watershed Using Hyperspectral Imagery and LiDAR

by

Mingquan Chen

Wildfire is a serious threat to millions of people living in the Western United States, yet also an integral part of Southern California ecosystems. Therefore, it is important to quantify fire impacts and patterns of post-fire landscape recovery in order to understand the links between fire events and ecosystems. This research combined Airborne Visible/Infrared Imaging Spectrometer (AVIRIS) remote sensing imagery and Light Detection and Ranging (LiDAR) data to produce a comprehensive, multi-year analysis of the May 2009 Jesusita Fire landscape within the Mission Creek Canyon watershed in Santa Barbara, California, USA. Combining passive and active remote sensing datasets allowed for a more detailed analysis of fire severity and the post-fire landscape recovery. Passive hyperspectral data provided information for a spectrally based assessment of fire severity and for mapping land cover types, while LiDAR provided geometric information such as topography and above ground vegetation structure. The study proposed a new fire severity definition based on multiple

hyperspectral and LiDAR metrics: Multiple Endmember Spectral Mixture Analysis (MESMA) fractions and differenced Normalized Burn Ratio (dNBR) from AVIRIS; and a Canopy Height Model (CHM) from LiDAR. The study also examined the topographic effects on fire severity and post-fire recovery, using a LiDAR derived Topographic Wetness Index (TWI) and riparian areas defined from river locations collected from fieldwork. The result showed that the dNBR-MESMA-CHM based severity definition depicted a more detailed severity distribution in the Jesusita fire scar compared to the traditional spectral fire indices, especially for those areas with significant amounts of dead trunks. The riparian zone or areas with high soil water content were less affected by the fire, and the level of green vegetation cover returned to pre-fire status earlier compared to the fire scar average.

TABLE OF CONTENTS

I. Introduction

A. Background

Wildfires are often viewed to be harmful to ecosystems but modern ecological research has shown that fire is an integral component in the function and biodiversity of many natural habitats. Thus, fire is now regarded as a natural disturbance (Keddy, 2007). Different ecosystem types in the United States have a characteristic frequency of fire ranging from once every 10 to 500 years (Brown & Smith., 2000). Fires are one of the most significant sources of disturbance in Mediterranean ecosystems (Moreno & Oechel, 1991; White et al., 1997) with a natural burn return interval of 20 to 100 years (Davis & Michaelsen, 1995). Native vegetation is widely considered adapted to fires, and some of them can grow back naturally from the root crown even after all above-ground vegetation is burned (Hanes, 1977). Ecological influences of wildfire can be divided into fire severity (short-term) and ecosystem response (long-term). Fire severity, or burn severity, is a measure of the magnitude of the effect that a wildfire has on the environment during the event (Keeley, 2009). The ecosystem response is referred to as the post-fire recovery of the ecosystem, such as vegetation growth (Bastos, Gouveia, Dacamara, & Trigo, 2011; Chen et al., 2011; Schimmel & Granstrom, 1996). Both fire severity and post-fire recovery can be affected by topography, soil wetness, precipitation etc. As wildfires often cover large areas with limited accessibility, satellite remote sensing is essential for gathering and analyzing spatial information, enabling the assessment of fire severity and post-fire recovery without extensive field sampling (Chu & Guo, 2014; Chuvieco, 2009; French et al., 2008; Miller & Yool, 2002).

Remote sensing technology can be divided into passive and active sensors. Passive sensors, i.e. multi-spectral and hyperspectral images, have been used to track burn severity (van Wagtendonk, Root, & Key, 2004) and changes in vegetation (Riano et al., 2002; White, Ryan, Key, & Running, 1996) on a spectral signal basis. Spectral indices, e.g. normalized difference vegetation index (NDVI) and Normalized Burn Ratio (NBR), have been used extensively to assess fire severity and post-fire recovery (Escuin, Navarro, & Fernández, 2008; García & Caselles, 1991; Veraverbeke, Lhermitte, Verstraeten, & Goossens, 2011, 2010). Methods based on a change in land cover composition also exist, since they have actual physical meaning and are easier to interpret than spectral indices (Adams et al., 1995). As the fire environment typically consists of a mixture of vegetation and ash, techniques that solve the mixed pixel problem are required (Kokaly, Rockwell, Haire, & King, 2007). Linear spectral mixture analysis (LSMA), the most widely used method, assumes measured reflectance of a mixed pixel is a linear combination of the spectra of each endmember (Riano et al., 2002; Roberts, Smith, & Adams, 1993; Röder, Hill, Duguy, Alloza, & Vallejo, 2008; Sankey, Moffet, & Weber, 2008; Smith, Lentile, Hudak, & Morgan, 2007; Souza, Firestone, Silva, & Roberts, 2003; Vila & Barbosa, 2010). LSMA is also able to estimate fractional cover of green vegetation, dead vegetation and soils in the fire scar, which is very similar to traditional field severity assessment (Lentile, Holden, Smith, Falkowski, & Hudak, 2006). Accuracy of LSMA mainly depends on the endmembers selection (Tompkins, Mustard, Pieters, & Forsyth, 1997). The number of endmembers must account for the number of classes in the pixel, which could vary on a per pixel basis. The same material could also have different spectral response in different pixels, thus using a single spectrum for each endmember class is potentially problematic. Multiple Endmember Spectral Mixture Analysis

(MESMA) can solve this issue by allowing multiple endmembers for each endmember class, and decomposing each pixel with a different combination of endmember (Quintano, Fernández-Manso, & Roberts, 2013; Roberts et al., 1998).

However, passive remote sensing data cannot directly provide any geometric properties of the topography or the above ground canopy, which leaves parts of the wildfire geography unexplored. For example, a trunk with crown mortality after fire will probably be detected as "ash or char" by hyperspectral imagery due to the reflectance of its burned surface. The ground topography information could also be difficult to extract in areas with certain levels of canopy density, since the reflecting feature could be largely blocked by above ground vegetation structures. This problem can be solved by using active sensors such as airborne LiDAR (light detection and ranging), which can measure accurate geometric X, Y, and Z position of reflecting surfaces. This includes measurements of the forest canopy and ground surface by high density laser pulses (Casas et al., 2016; Kane et al., 2010; Lefsky, Cohen, Parker, & Harding, 2002; Lefsky, Turner, Guzy, & Cohen, 2005). Thus, the combination of multiple types of remote sensing data will provide better opportunities for scientific analysis (Hyde et al., 2006). As LiDAR often lacks area coverage and is expensive for operation, topography and surface structures are not widely considered in fire analysis, leaving many questions unanswered regarding the relationship between wildfire and topography.

B. Motivation

In Santa Barbara, California, wildfires have been frequent, with major wildfires occurring as frequently as nine years or less in the Santa Ynez Mountains since the 1955 Refugio Fire. Moreover, more than five of the major wildfires have burned in the last decade, including the

Gap, Tea and Jesusita Fires. Hyperspectral data are available over these fires on multiple dates before and after the fire, while airborne LiDAR covered parts of the Jesusita fire scar after the event.

In this study, both hyperspectral imagery and LiDAR were combined to produce a comprehensive, multi-year analysis of the post-fire landscape within the Mission Creek Canyon watershed. With these datasets, we were able to analyze changes to both the land cover and watershed structure in the years following the fire. The research goals are: 1) combine hyperspectral and LiDAR data to produce a more detailed fire severity definition compared to the traditional spectral index based version; 2) understand how topography affected fire severity and vegetation survival; 3) understand how topography influenced post-fire recovery.

II. Materials

A. Study Area

The study is focused on the Jesusita Fire, which began at approximately 1:45 PM on May 5, 2009 in the hills of Santa Barbara, California at 34°27' N -119°43' W (Figure II-1). The fire burned 35.40km^2, destroyed 80 homes and damaged 15 more before being fully contained[1]. Santa Barbara has a typical Mediterranean climate with hot, dry summers and cool wet winters. Seasonal temperature variation is moderate and annual precipitation is low. Elevational changes range from sea level to 1310 m along the crest of the Santa Ynez Mountains. The east–west orientation of the mountains and its dramatic variation in elevation produce a highly contrasting environment, resulting in a significant vegetation diversity (Roberts, Dennison, Roth, Dudley, & Hulley, 2015). Dominant vegetation consists of a mixture of open grassland, oak savannas, open pine forest and shrubland.

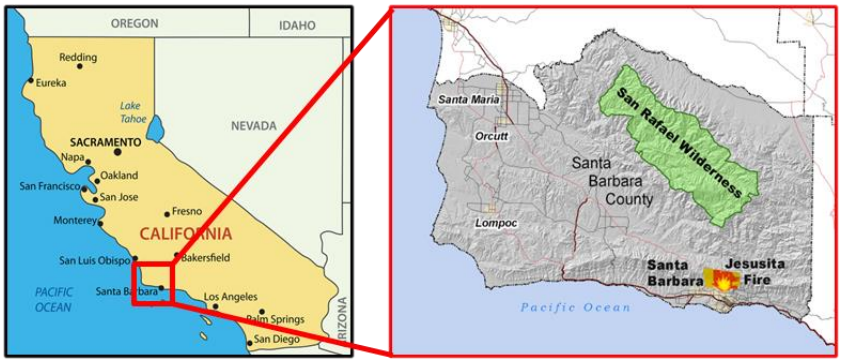

Figure II-1: Location of Jesusita Fire.

[1] "Jesusita Fire" from CAL FIRE Archive (https://web.archive.org/web/20160304022718/http:/cdfdata.fire.ca.gov/incidents/incidents_details_info?incident_id=310).

The Study site can be divided into two parts: the whole fire scar and surrounding area that is covered by the Airborne Visible/Infrared Imaging Spectrometer (AVIRIS) and the eastern part of the fire scar in the Mission Creek and Rattlesnake Canyon Watershed, which were covered by LiDAR (Figure III-1).

B. Remote Sensing Data

1. Hyperspectral Data

AVIRIS is an airborne optical sensor that delivers calibrated images of the upwelling spectral radiance in 224 contiguous spectral bands with wavelengths from 400 to 2500 nm (Green et al., 1998). It was deployed on the ER-2 aircraft, and the flight line covered most of the Jesusita fire scar and its surroundings. The raw AVIRIS data were processed to surface reflectance using MODTRAN (Roberts, Green, & Adams, 1997). Retrieved reflectance was further corrected for minor artifacts using a field measured spectrum of a beach sand target present on the southern flight lines (Clark et al., 2002). Prior to further analysis, strong water vapor bands centered at1400 nm and 1900 nm were removed. The data were then georeferenced using a Digital Orthophoto Quarter Quads (DOQQ) as a base image, with a second order polynomial transformation and nearest neighbor sampling. The data were acquired at different spatial resolutions on different dates (Table II-1), and were standardized to a uniform 12-meter spatial resolution for further analysis.

Table II-1: Acquired date and spatial resolution of the AVIRIS data (http://aviris.jpl.nasa.gov/index.html).

Acquisition Date	Flightline	Solar Zenith (º)	Solar Azimuth (º)	Resolution (m)	Pre-Fire	Post-Fire
Mar-09	f090330t01p00r08	30.61	181.87	12	✓	
	f090330t01p00r09	31.42	194.19			
Jun-09	f090617t01p00r06	12.16	205.17	12		✓
	f090617t01p00r08	17.88	236.07			
Aug-09	f090826t01p00r09	30.22	221.63	12		✓
	f090826t01p00r10	32.80	228.53			
Apr-10	f100430t01p00r05	26.66	132.69	12		✓
	f100430t01p00r07	21.88	151.06			
Jul-11	f110719t01p00r09	51.00	186.35	7.5		✓
	f110719t01p00r10	51.80	192.72			
Apr-13	f130411t01p00r10	26.54	184.15	18		✓
	f130411t01p00r12	28.98	207.68			
Jun-13	f130606t01p00r08	12.20	170.67	18		✓
	f130606t01p00r14	30.57	256.33			

2. LiDAR Data

The Lidar data were collected using an airborne Lidar sensor in December 2009 and August 2010 after the Jesusita Fire had burned (Figure II-2.A). Imagery was acquired over an area of 15,530,802 m^2 in 2009 and 69,942,152 m^2 in 2010 with a point density of 30-40 points/m^2, which overlaps with the eastern part of the fire scar.

In order to preprocess the LiDAR point cloud data, a Python wrapper script was used to implement LAStools (http://www.cs.unc.edu/~isenburg/lastools/). First, duplicate LiDAR points were removed, and then the whole point cloud dataset was split into tiles smaller than 250MB to make it more manageable. Feature detection was applied to the raw point cloud tiles to classify them into buildings, ground, and vegetation points based on specific thresholds. Then the ground points were gridded into raster using Triangulated Irregular

Network (TIN) interpolation, which creates the Digital Elevation Model (DEM). Similarly, vegetation point heights above ground are calculated and gridded into the Canopy Height Model (CHM). Both DEM and CHM raster images were created with 1-meter pixel resolution (Figure II-2.B).

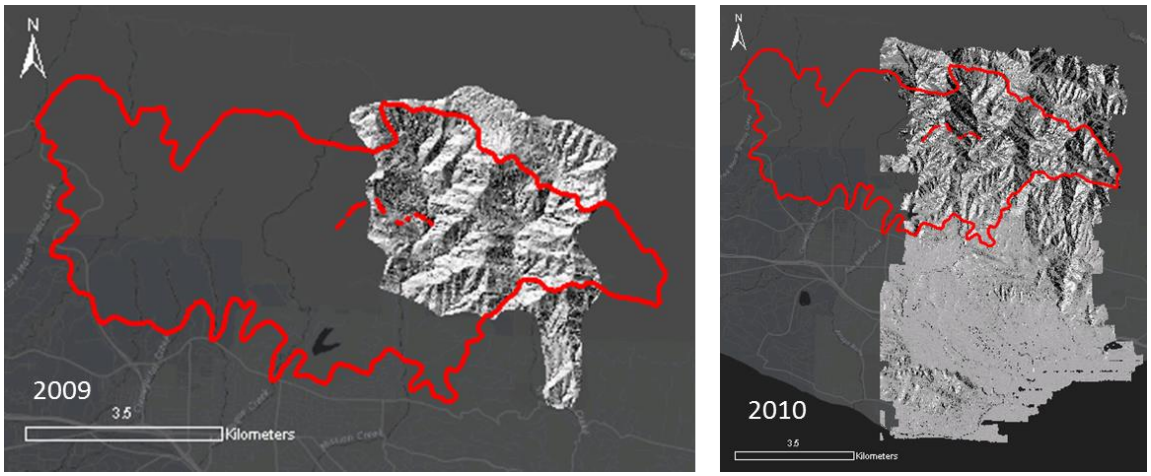

(A)

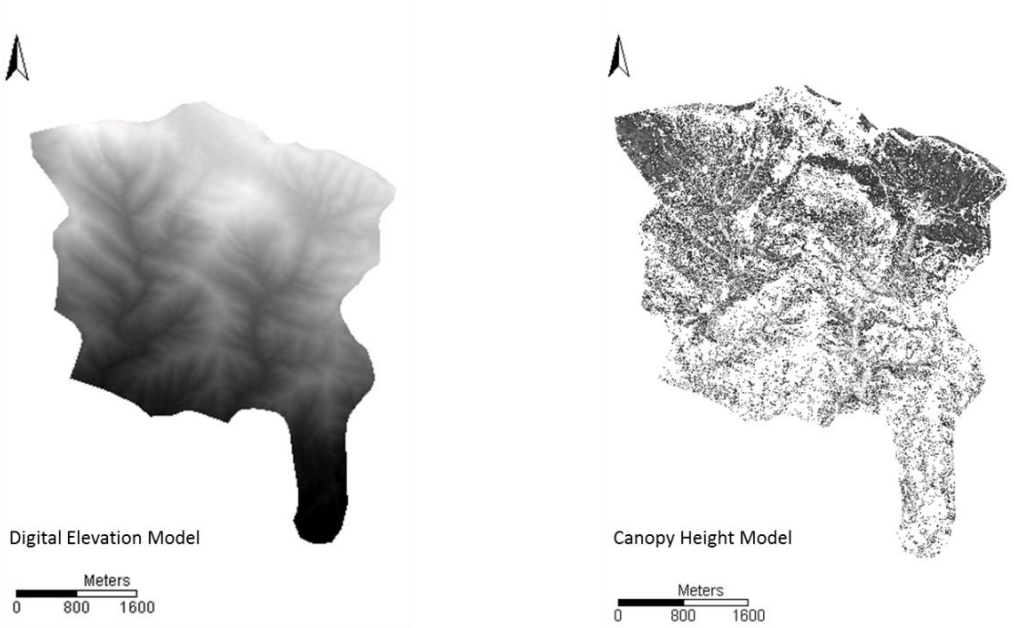

(B)

Figure II-2

A: Lidar data coverage is shown as a hillshade layer, with the red boundary representing the final fire boundary; B: Digital Elevation Model and Canopy Height Model extracted from the 2009 LiDAR dataset.

III. Methods

The methods proposed in this study can be divided into three parts (Figure III-1). Detailed procedures (Figure III-2) will be provided in later sections.

- LiDAR related data processing: this covers part of the eastern Jesusita fire scar area and adjacent area outside the fire scar. Data outside of the Mission Creek Canyon watershed is excluded for watershed analysis.
- AVIRIS related data processing: this covers the whole Jesusita Fire region, and is available on multiple dates both pre-fire and post-fire.
- Data fusion analysis: LiDAR image and AVIRIS image are stacked together for fusion analysis.

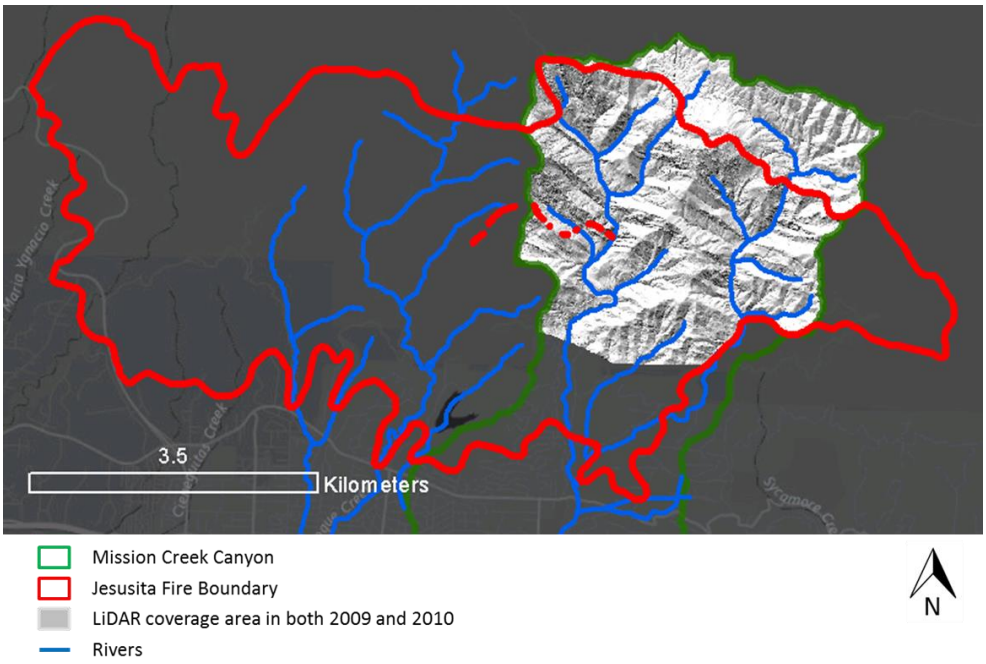

Figure III-1: Data coverage of AVIRIS and LiDAR sensor over the Jesusita fire area that is included in this research. The whole fire scar and its surrounding area are covered by AVIRIS. LiDAR covers the red part of the fire scar and green part outside the fire scar.

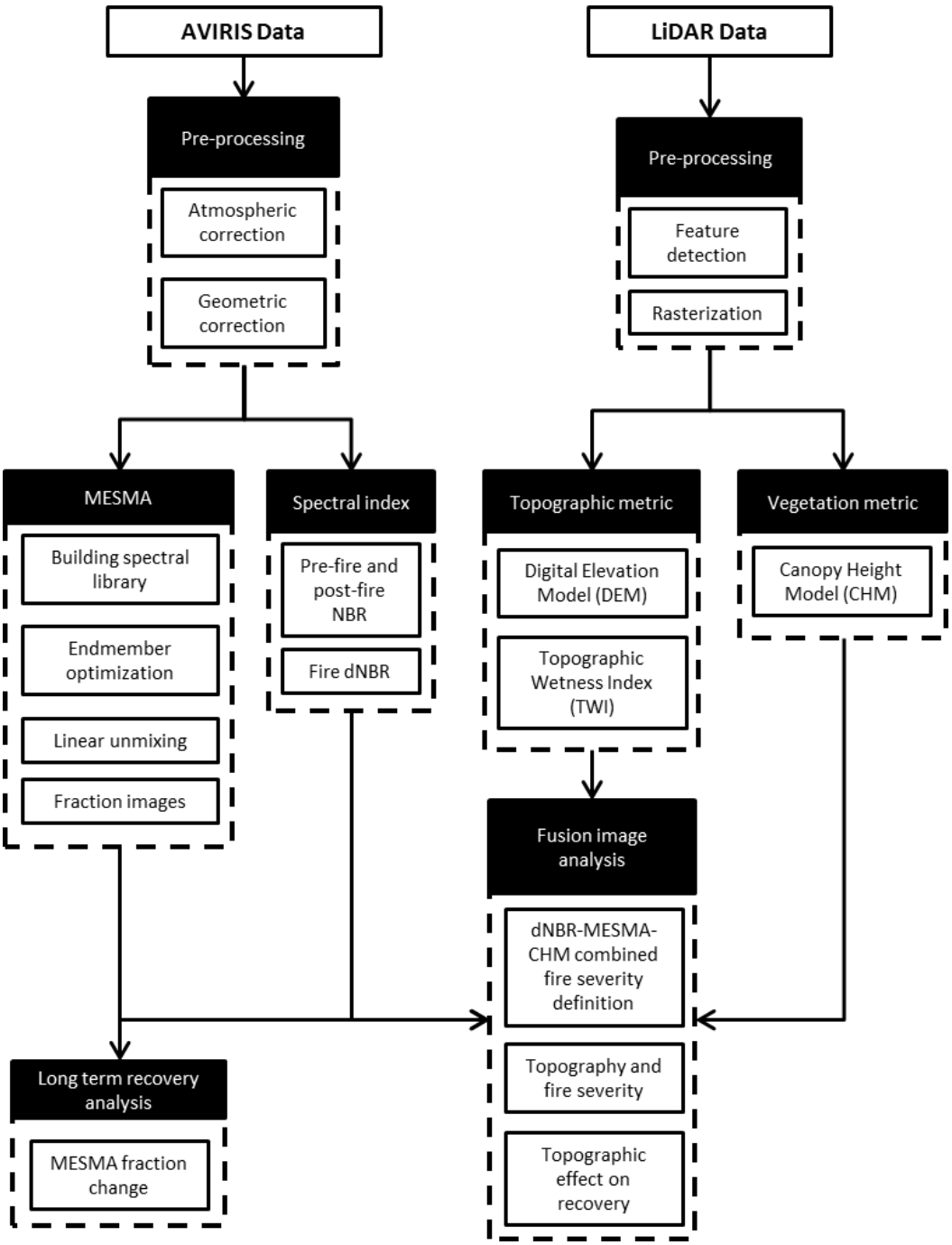

Figure III-2: Flow chart of processing approach.

A. NBR Based Fire Severity

Remote sensing data have been used to calculate NBR with near-infrared and short-wave infrared bands (Escuin et al., 2008). The temporal difference between the pre- and post-fire NBR values is called the differenced Normalized Burn Ratio (dNBR), which represents the burned area from unburned surroundings by a scaled index of the change caused by fire. The dNBR is widely used to assess landscape-level fire severity (Lutes et al., 2007). Hyperspectral data, such as that provided by AVIRIS, have been used to validate assumptions about the response sensitivity of Landsat bandwidths to burn severity (van Wagtendonk et al., 2004). NBR for AVIRIS is calculated using band 47 and 210 at wavelength of 788 and 2370 nm as:

$$NBR_{AVIRIS} = \frac{R_{47} - R_{210}}{R_{47} + R_{210}}$$

While dNBR for burn severity is calculated as:

$$dNBR_{AVIRIS} = NBR_{pre} - NBR_{post}$$

The reflectance differences in each channel quantified the spectral response over the time interval and indicated the degree of spectral change due to the fire. Temporal response in apparent reflectance was measured from pre-fire to post-fire for high severity, moderate severity, low severity, and unburned areas. These four severity regions are mainly used for grouping pixels for comparison, not as a rigorous a priori definition of the severity.

The images used for dNBR calculation were 03/2009 and 08/2009. Ranges of different levels of burn severity were selected based on USGS FIREMON (Lutes et al., 2007). The severity levels are somewhat flexible with a shift of 0.01 to 0.1, due to the image-timing factor. When

the post-fire scene is drier than the pre-fire scene, the burn-unburned threshold tends to increase because of phenology. There is also considerable confusion between low severity burned pixels and dry unburned pixels (Lutes et al., 2007). This is actually the case for a Mediterranean climate with a dry 2009 summer. The dNBR in north Mission Creek Canyon outside of the fire scar was also calculated, where no fire occurred three years prior to Jesusita Fire (Figure III-3). As can be observed in the histogram, non-fire related changes caused the dNBR to increase by 0.1. As a result, the upper end of the unburned category was raised from 0.1 to 0.2 for this study (Table III-1).

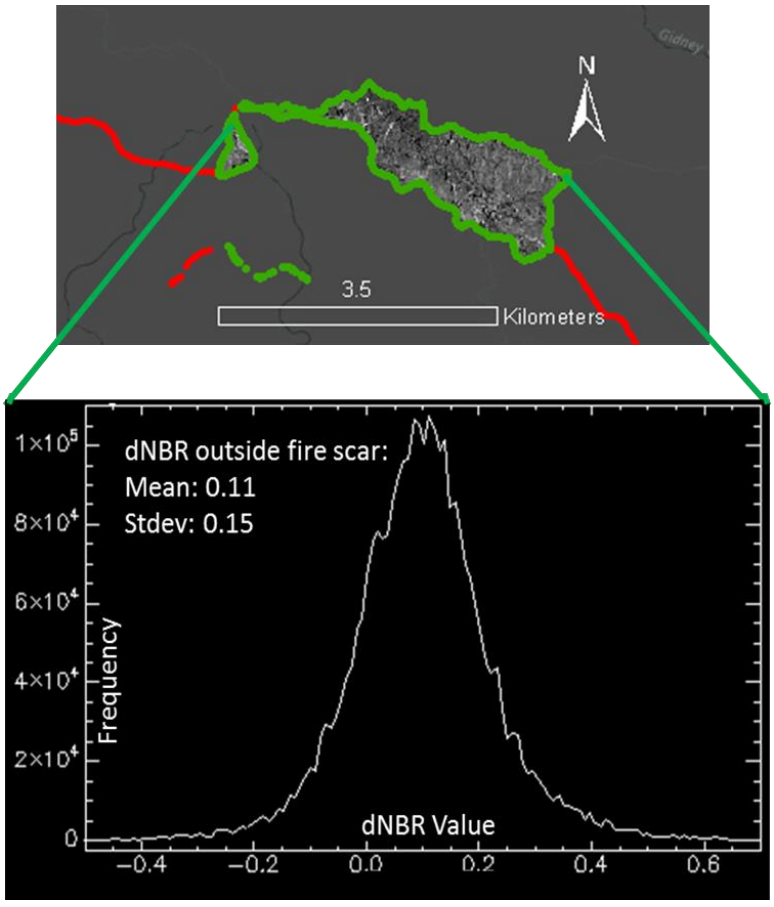

Figure III-3: dNBR outside Jesusita Fire, which reveals the NBR value change result from phenology factor rather than wildfire.

Table III-1: The original dNBR levels definition (Lutes et al., 2007) and the modified levels with corresponding dNBR value.

Original dNBR Level	Modified dNBR Level	Burn Severity
-0.5 to 0.1	-0.4 to 0.2	Regrowth or Unburned
0.1 to 0.27	0.2 to 0.37	Low Severity burn
0.27 to 0.66	0.37 to 0.76	Moderate Severity burn
0.66 to 1.2	0.76 to 1.3	High Severity burn

Within the Mission Creek and Rattlesnake Canyon watershed, the 2009 Jesusita Fire event can be clearly detected using AVIRIS. Following the fire, the watershed largely transformed into high severity fire scar (Figure III-4). A visual analysis indicates that riparian areas were more protected from the fire, with lower severity present after the event. Uplands appear more uniformly charred.

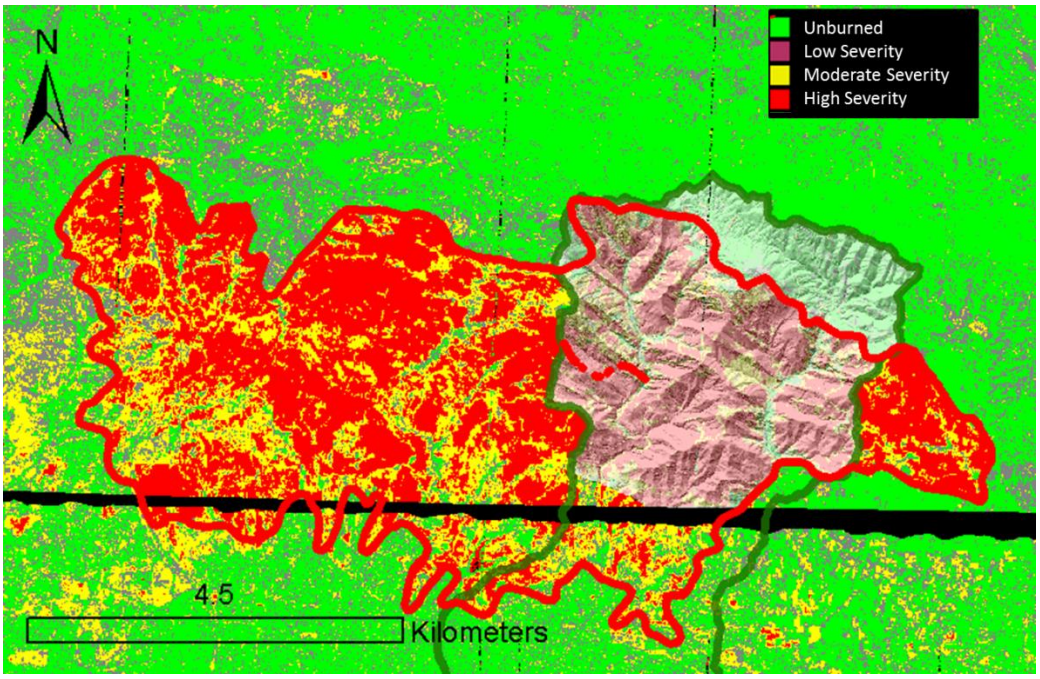

(A)

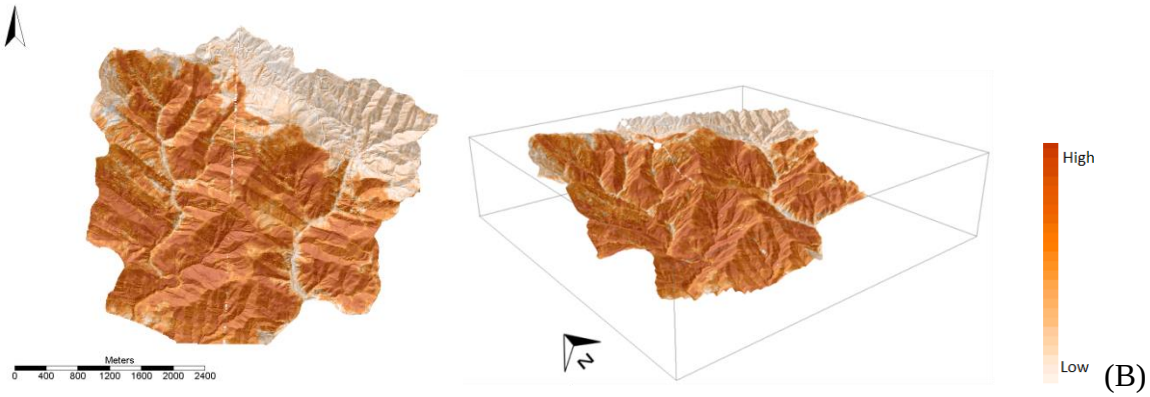

(B)

Figure III-4

A: Fire severity derived from dNBR. Most of the Jesusita fire scar is defined by high severity. The transparent hillshade area shows the LiDAR data coverage area. There is a gap with no data between the two AVIRIS flight lines.

B: A monochrome dNBR map overlaid on the whole LiDAR DEM, which shows pattern of the fire severity in terms of topography. The fire scar boundary matches well with the dramatic change in dNBR in the northern part of this map.

The dNBR indicates that more than 50% of the whole Jesusita fire scar area had high burn severity (Table III-2). The average burn level of the whole fire scar was less severe than the area covered by LiDAR.

Table III-2: Area percentage of different fire severity defined by dNBR in the whole Jesusita fire scar and LiDAR covered fire scar.

Burn severity level from dNBR	Whole fire scar (35.40 km^2)	LiDAR coverage in fire scar (9.75 km^2)
Unburned	7.03%	4.23%
Low	7.83%	4.88%
Moderate	34.40%	24.50%
High	50.74%	66.40%

B. MESMA Based Fire Severity

An AVIRIS image is likely to have a mixture of ground cover types with a spatial resolution of 7.5~18 meters. Traditional linear spectral mixture analysis (LSMA) only allows one spectrum for each endmember. MESMA resolves this restriction by allowing endmembers to vary on a pixel basis (Roberts et al., 1998). The capability of testing multiple models on each image pixel can map more land materials while minimizing pixel fraction errors by choosing the best-fit model for every single pixel. Regarding the focus or fire burn severity in this study, the endmembers used included green vegetation (GV), non-photosynthetic vegetation (NPV), ash and soil. The MESMA procedure here consisted of three steps: 1) building a spectral library from AVIRIS images; 2) endmember optimization for the final spectral library; 3) AVIRIS image unmixing. All of these approaches were done with the Visualization and Image Processing for Environmental Research (VIPER) tools software (Quintano et al., 2013; D. Roberts, Halligan, & Dennison, 2007; Veraverbeke et al., 2012).

1. Building the spectral library:

The spectra retrieved from the AVIRIS image were used as endmember candidates (image endmember). Considering phenological variability present in images acquired over different dates, two libraries with ash, GV, NPV and soil were developed: a spring library from June 2009 that was applied to images between March and June, and a summer library from August 2009 applied to July to November images.

2. Endmember optimization:

The accuracy of a mixing model depends highly on the quality of endmembers (Tompkins et al., 1997). In this study, three techniques were applied to identify those candidate endmember spectra that are most representative of a specific class and least likely to confuse with a different class. These methods included: 1) Count- based Endmember Selection (CoB): endmembers are selected that model the greatest number of endmembers within their class (Roberts et al., 2003). 2) Endmember Average RMSE (root mean squared error) (EAR): endmembers are selected that produce the lowest RMSE within a class (Dennison & Roberts, 2003a, 2003b); and 3) Minimum Average Spectral Angle (MASA): endmembers are selected that have the lowest average spectral angle (Dennison, Halligan, & Roberts, 2004). After the optimization process, each ground cover type in each library had less than or equal to six sample spectra (Figure III-5).

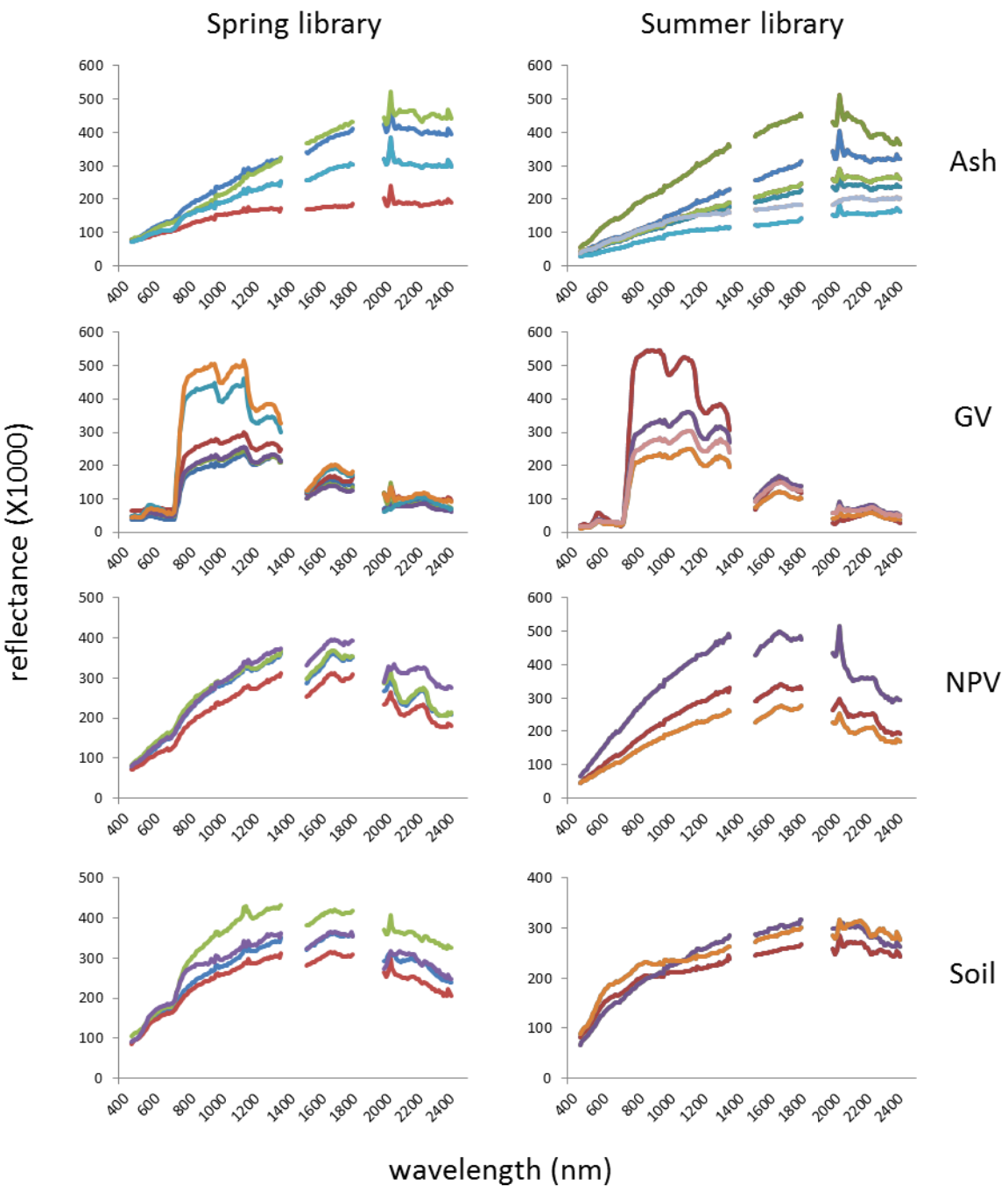

Figure III-5: Endmembers spectra of spring and summer library derived from AVIRIS image acquired on June 2009 and August 2009, respectively.

3. AVIRIS image unmixing:

Every pixel in the AVIRIS image was modeled as a linear combination of the four fractional-cover types mentioned previously: GV, NPV, ash and soil (Quintano et al., 2013). The images were unmixed into those fractions and shade using MESMA. The criteria of selections were: 0 and 1 as the minimum and maximum permissible fraction values; 0.8 as maximum permissible shade fraction value, and 0.025 as maximum permissible RMSE (Roberts, Quattrochi, Hulley, Hook, & Green, 2012; Roberts et al., 2003). Multiple models were tested on a pixel basis, and the model with the lowest RMSE was selected. A pixel would be marked as unclassified if the RMSE exceeded the threshold.

C. DEM Based Soil Surface Moisture Model

Topographic features may influence surface runoff, subsurface water movement, the development of zones of surface saturation, and the distribution of soil water content across a catchment (Chirico, Western, & Grayson, 2005; Moore, Burch, & Mackenzie, 1988; Western, Grayson, Bschl, & Willgoose, 1999; Zaslavsky, 1981). The topographic wetness index (TWI), which combines local upslope contributing area and slope, is commonly used to quantify topographic control on hydrological processes (Beven & Kirkby, 1979; Moore, Grayson, & Ladson, 1991). In many cases, it is not possible to carry out direct measurements of these environmental processes because of physical, time, or economic constraints. If elevation data are accessible through LiDAR, topographic attributes can be readily calculated without these constraints. TWI, a unitless index that estimates soil water content and surface saturation zones, can be calculated from a DEM as:

$$w = \ln(\frac{A_s}{tan\beta})$$

Where A_s is defined as the upslope area draining across a unit width of contour. It measures surface or shallow subsurface runoff at a given point on the landscape, which integrates the effects of upslope contributing area, together with catchment convergence and divergence on runoff; β is slope.

First, the DEM was aggregated to 12-meter resolution to remove delicate sinkholes and depressions, and the TWI was generated based on that (Figure III-6). The pattern of the TWI image matches the actual river map acquired from the Santa Barbara Coastal Long Term Ecological Research (SBC LTER: http://sbc.lternet.edu/) well, especially for those area with high TWI. Moreover, it provides more detail of the estimated soil moisture based on the local topography.

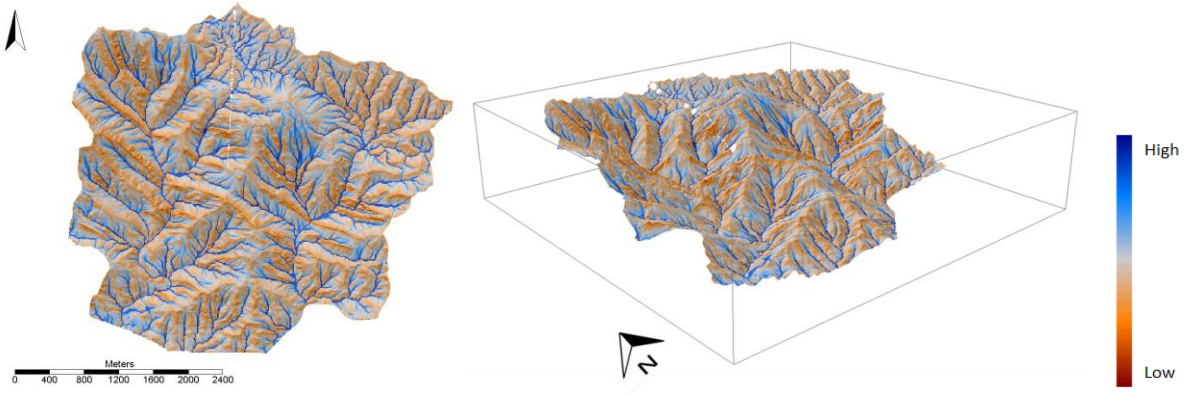

Figure III-6: 3D visualization of the 2009 DEM derived TWI.

D. Data Fusion Approach

Data fusion deals with association, correlation, and combination of information and data from different sources. In this study, data derived from both AVIRIS and LiDAR were

integrated into a single image for further analysis (Figure III-2). Since the airborne LiDAR did not cover the whole fire scar area, only the area within the Mission Creek Watershed that overlapped with the LiDAR area in 2009 is included (Figure III-1). These AVIRIS image and LiDAR data were not collected on the exact same day. However, there was not enough precipitation during that time gap to greatly change the landscape or produce significant biomass increase, and very little growth typically takes place prior to October due to dry summers (Table III-3). Therefore, it is legitimate to treat the LiDAR derived CHM as if it was acquired on the same date as AVIRIS. Precipitation and fog data were collected from Coal Oil Point Reserve (http://www.geog.ucsb.edu/ideas/) which lies 25 km to the west of Mission Creek (Roberts, Bradley, Roth, Eckmann, & Still, 2010). As for the TWI, the average change from 2009 to 2010 (first year after the fire event) in the LiDAR fire scar was 0.001, with 60.92% of the pixels remaining unchanged. So, the 2010 TWI was also used for AVIRIS images later than 2010.

The fusion images included are the four MESMA fraction bands, the dNBR band, and the two LiDAR rasterized images CHM and TWI (Figure III-7). Three different fusion images for different dates were created based on data availability (Table III-4). All pixels were resized to 1m resolution, and projection converted to NAD83 / UTM zone 11N.

The next chapter will focus on integrating those hyperspectral and LiDAR based metrics. The CHM will be an extra input for the dNBR and MESMA for detecting dead trunks, also extending the traditional dNBR based fire severity definition. The TWI would be an indicator to examine how soil water content could affect the fire severity and post-fire recovery process.

Table III-3: The amount of precipitation and fog moisture accumulation between the gap of AVIRIS and LiDAR acquisition in 2009 and 2010.

Year	AVIRIS Date	LiDAR Date	Precipitation (mm)	Fog (mm)
2009	August	December	138.938	56.1
2010	October	August	69.858	30.2

Table III-4: Components of fusion images.

Fusion Image	MESMA	dNBR	CHM	TWI
2009 Image	✓	✓	✓	✓
2010 Image	✓	X	✓	✓
2009 - 2013 time series image	✓	X	X	✓

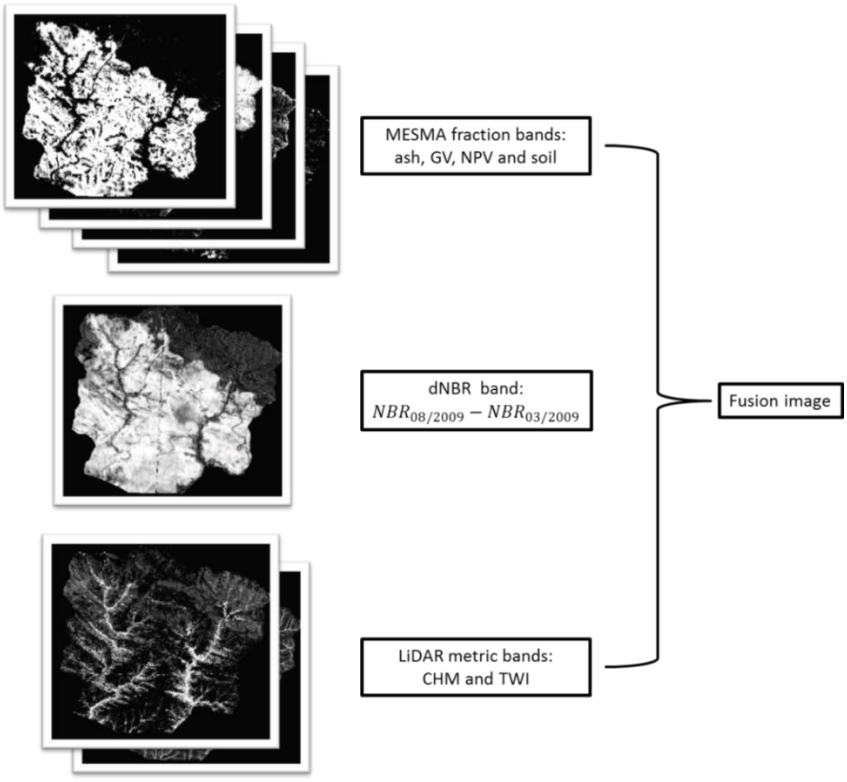

Figure III-7: The fusion image bands.

IV. Results and Discussion

A. A dNBR-MESMA-CHM Combined Fire Severity Definition

In addition to the spectrally based fire severity alone (Table IV-1), the CHM derived from LiDAR data provides information on vegetation height metrics. A comparison was made between the dNBR level and CHM values both inside and outside of the fire scar area (Figure IV-1, A and C). Note that elevated dNBR outside of the fire scar does not indicate the existence of fire, but acts as a control group and quantifies the impact of phenology on dNBR. The Mediterranean summer dryness was a major contributor to elevated severity both inside and outside the fire scar, which requires a control group. The plants outside the fire scar that showed moderate or high dNBR are probably drought deciduous shrubs, such as coastal sage, which senesces between March and August (Harrison, Small, & Mooney, 1971).

Table IV-1: A summary of area with different dNBR level inside and outside the fire scar covered by LiDAR. The "burn" outside fire scar is more of an artifact caused by phenological dryness during summer, although a small portion of that could be caused by ash flowing away from the fire event.

LiDAR coverage area	Inside fire scar: 9,731,319m^2		Outside fire scar: 2,924,970m^2 (control group)	
	Area (m^2)	Area (%)	Area (m^2)	Area (%)
Unburned dNBR	411,542	4.23%	2,396,387	81.93%
Low dNBR	474,766	4.88%	452,568	15.47%
Mod dNBR	2,383,732	24.50%	74,545	2.55%
High dNBR	6,461,279	66.40%	1,302	0.04%

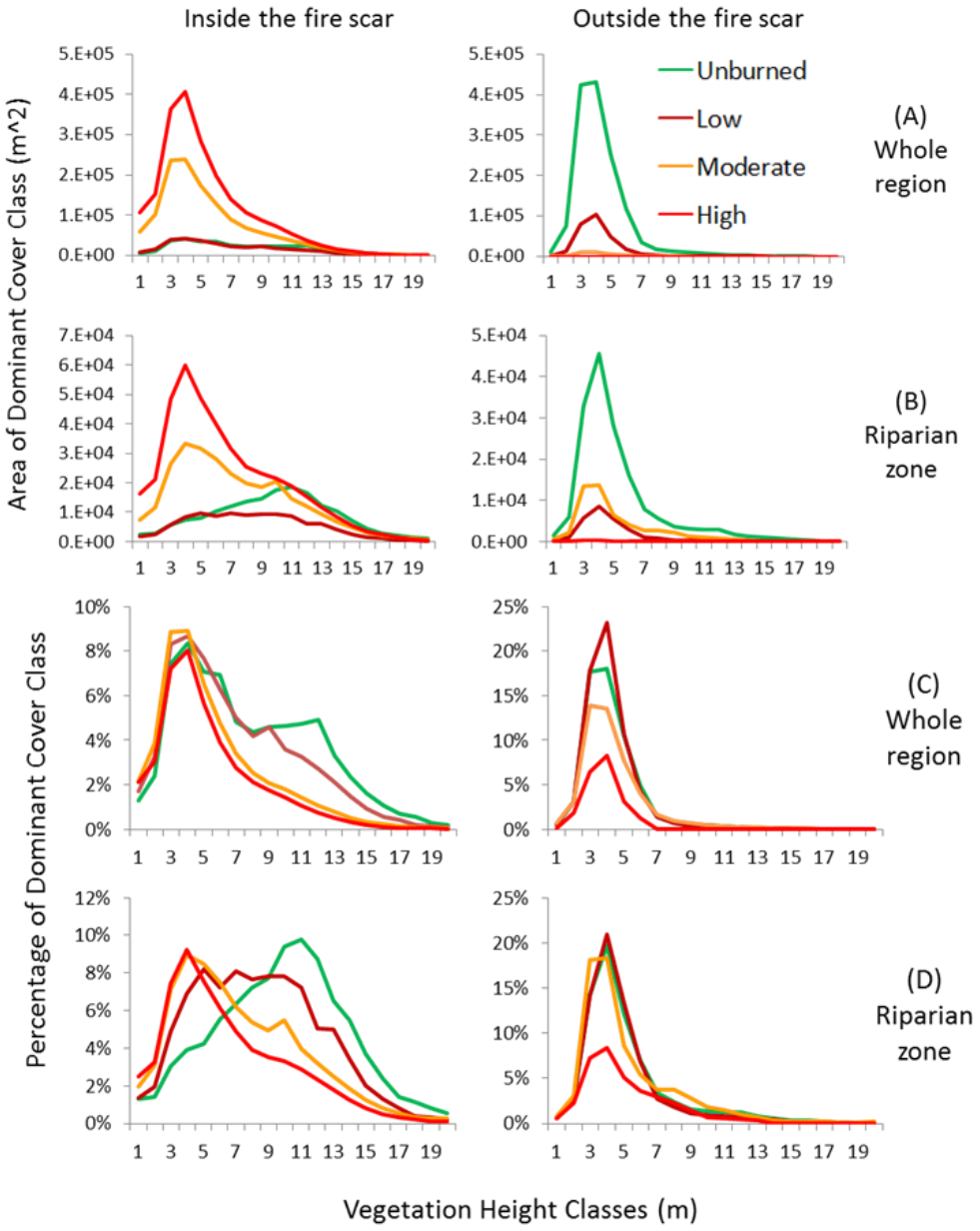

Figure IV-1: Different CHM heights and its corresponding dNBR level within LiDAR covered places. Statistics are presented in percentage and actual cover area in m^2. Results are divided into area inside and outside the fire scar, the whole region (A and C) and riparian zone (B and D). The definition of riparian zone is discussed in section IV-B (Figure IV-6).

These statistics show that the fire scar was dominated by a high dNBR level. In addition, a certain portion of high dNBR area retained above ground vegetation structure after the fire, including trunks taller than 10m. The area outside of the scar was mostly unburned, with minor areas of low and moderate dNBR caused by phenological dryness. Similar patterns can be observed in the comparison between MESMA fractions and CHM in 2009 (Figure IV-2, A and C), where a certain amount of vegetation structure remains in ash-dominated places.

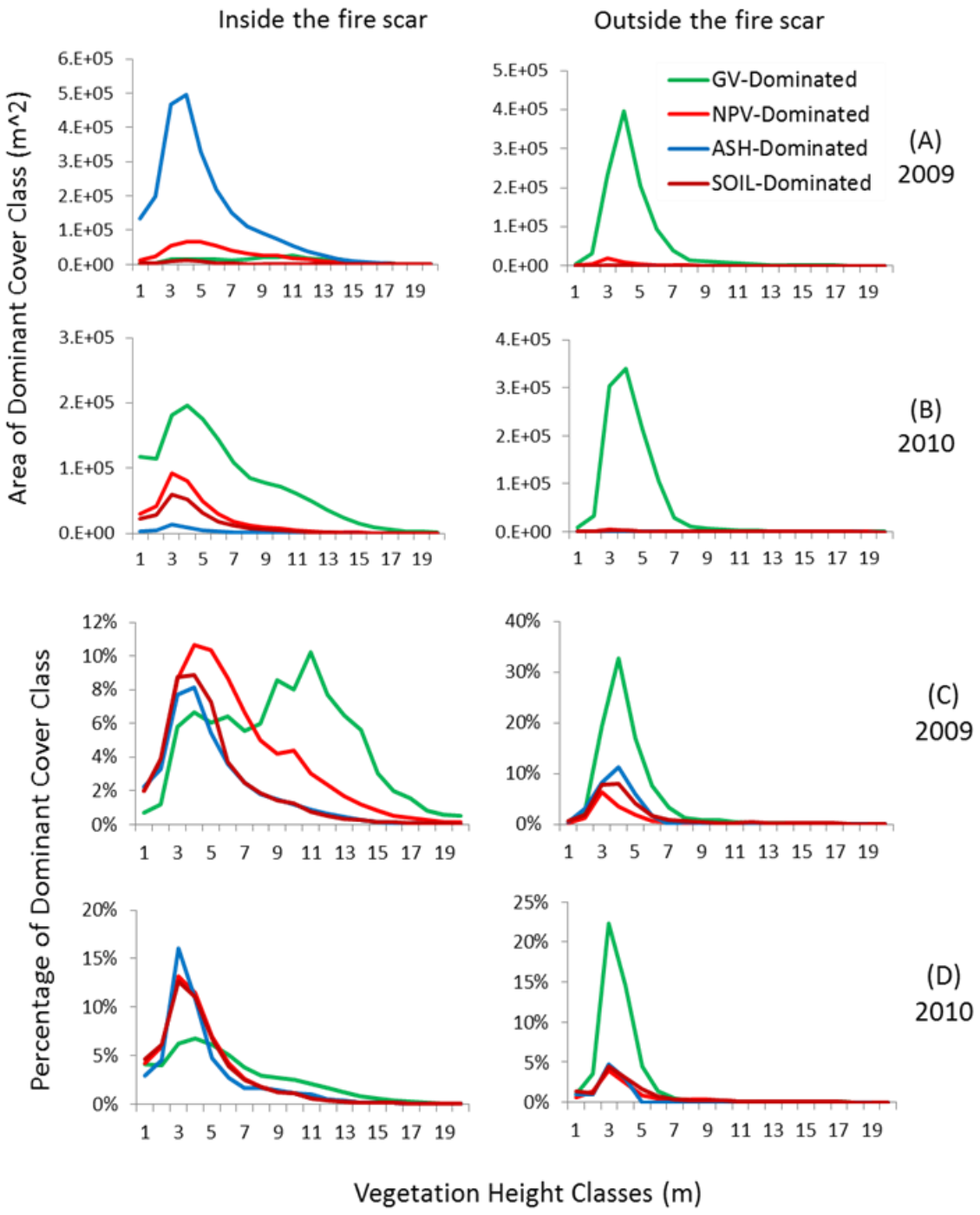

Figure IV-2: Different CHM heights and its corresponding MESMA domination type within LiDAR covered places in both 2009 (A and C) and 2010 (B and D). Statistics are presented in percentage and actual cover area in m^2. "Domination" is defined by more than 75% more a certain fraction type. Ash with zero CHM is excluded in the chart.

A typical height of Chaparral species in California is around 5m. If 5m is set as a threshold for the CHM, many pixels in the fire scar taller than this threshold are still dominated by ash or recorded as high burn severity in dNBR. However, the portions of those that exceed the 5m threshold and have high burn severity consist of less than 1% outside of the fire scar (Table IV-2). The distribution of pixels that meet all the three criteria, i.e. ash dominated, high dNBR and CHM > 5m, are heavily concentrated adjacent to the riparian zone and its adjacent valley, i.e. high TWI places (Figure IV-3).

Table IV-2: Percentage of pixels with CHM > 5m that are dominant by ash or with high dNBR.

	Inside scar (m^2)		Outside scar (m^2)	
Total LiDAR coverage area	9,731,319		2,924,970	
CHM > 5m, in ash dominated area	851,678	8.75%	55	0.00%
CHM > 5m, in high burn severity area	965,514	9.92%	17	0.00%
CHM > 5m, both ash dominated & high dNBR	775,323	7.97%		

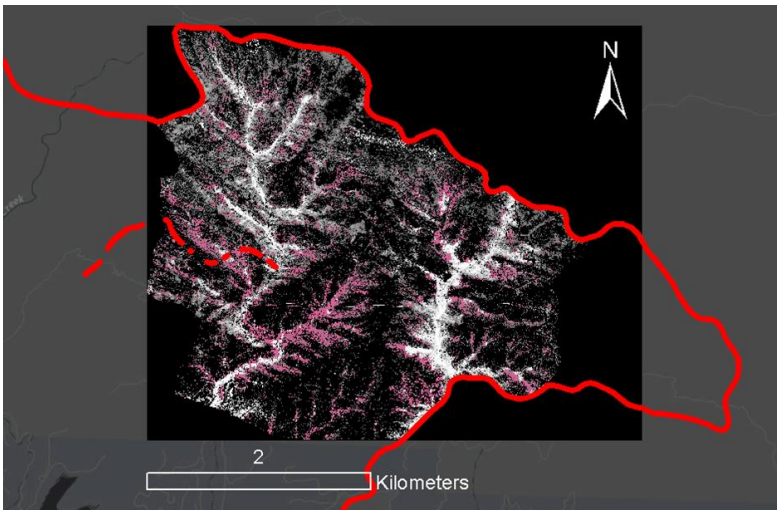

Figure IV-3: Distribution of pixels with CHM > 5m, ash dominated and high dNBR in the LiDAR covered fire scar area.

It is obvious that a certain amount of vegetation inside the fire scar is completely burned, but the trunk and branches remain above ground. Hyperspectral spectroscopy is not able to detect this alone without the CHM derived by LiDAR. A new method of burn severity definition is required to consider all those factors.

According to the dNBR-MESMA-CHM statistics (Table IV-3), the ash fraction in high dNBR area is high and consistent with a mean value of 0.945 and RSD (relative standard deviation) of 0.177. Moreover, the mean CHM of high dNBR pixels is the smallest (3.398m) among all dNBR levels, while the RSD is the highest (1.574), which quantifies the high variability of bare earth and dead trunks in the fire scar (Figure IV-1.C). In moderate dNBR area, the ash fraction is still high (mean 0.607, RSD 0.679) with large variation on CHM as well (RSD 1.386). As high and moderate dNBR consist of more than 90% of the area (Table IV-1), more detailed burn level separation is needed.

Also, a high severity does not guarantee a landscape is stripped of biomass, especially when that area was densely vegetated prior to the fire (Miller & Thode, 2007). As a result, a post-fire MESMA fraction map will be a significant input for the new fire severity map.

Table IV-3: Different dNBR level with its corresponding CHM and MESMA fraction statistics inside the fire scar covered by LiDAR.

	dNBR level	Unburned dNBR	Low dNBR	Mod dNBR	High dNBR
Mean	CHM (m)	5.354	4.226	2.680	2.159
	Ash	0.093	0.173	0.607	0.945
	GV	0.587	0.330	0.067	0.006
	NPV	0.266	0.398	0.255	0.042
	Soil	0.054	0.099	0.071	0.007
Standard deviation	CHM (m)	4.892	4.378	3.715	3.398
	Ash	0.226	0.290	0.412	0.167
	GV	0.331	0.302	0.149	0.031
	NPV	0.307	0.339	0.360	0.153
	Soil	0.166	0.244	0.206	0.055
Relative standard deviation	CHM	0.914	1.036	1.386	1.574
	Ash	2.430	1.676	0.679	0.177
	GV	0.564	0.915	2.224	5.167
	NPV	1.154	0.852	1.412	3.643
	Soil	3.074	2.465	2.901	7.857

Here, a new dNBR-MESMA-CHM based fire severity definition is proposed (Table IV-4). The high severity dNBR area with zero CHM and dominated by ash (ash fraction ≥ 0.75) is categorized as extreme severity due to the eradication of all vegetation structure above ground. As for moderate dNBR level, there is more ambiguity from the spectral perspective due to a mixture of ash and significant increase in NPV, which is a typical case for shrub crown mortality when CHM is larger than 0. In this case, the moderate level is divided into moderate-high (CHM = 0) and the moderate-low (CHM > 0). The fire map produced from this new severity definition (Figure IV-4) provided better level resolution for moderate and high severity.

Table IV-4: A dNBR-MESMA-CHM based fire severity definition and corresponding area of each fire severity level, as of August 2009. The "burn" outside fire scar is a control group as (Table IV-1).

dNBR-MESMA-CHM Severity	Criteria	Inside fire scar: 9,731,319m^2		outside fire scar: 2,924,970m^2 (control group)	
		Area (m^2)	Area (%)	Area (m^2)	Area (%)
Unburned	$-0.4 \leq dNBR \leq 0.2$	411,542	4.23%	2,396,387	81.93%
Low	$0.2 < dNBR \leq 0.37$	474,766	4.88%	452,568	15.47%
Mod-low	$0.37 < dNBR \leq 0.76$, CHM > 0	1,295,143	13.31%	41,625	1.42%
Mod-high	$0.37 < dNBR \leq 0.76$, CHM = 0	1,088,589	11.19%	32,920	1.13%
High	$0.76 < dNBR \leq 1.3$, Ash < 0.75 or CHM > 0	3,313,940	34.05%	1,148	0.04%
Extreme	$0.76 < dNBR \leq 1.3$, Ash $\geq$ 0.75, CHM = 0	3,147,339	32.34%	154	0.01%

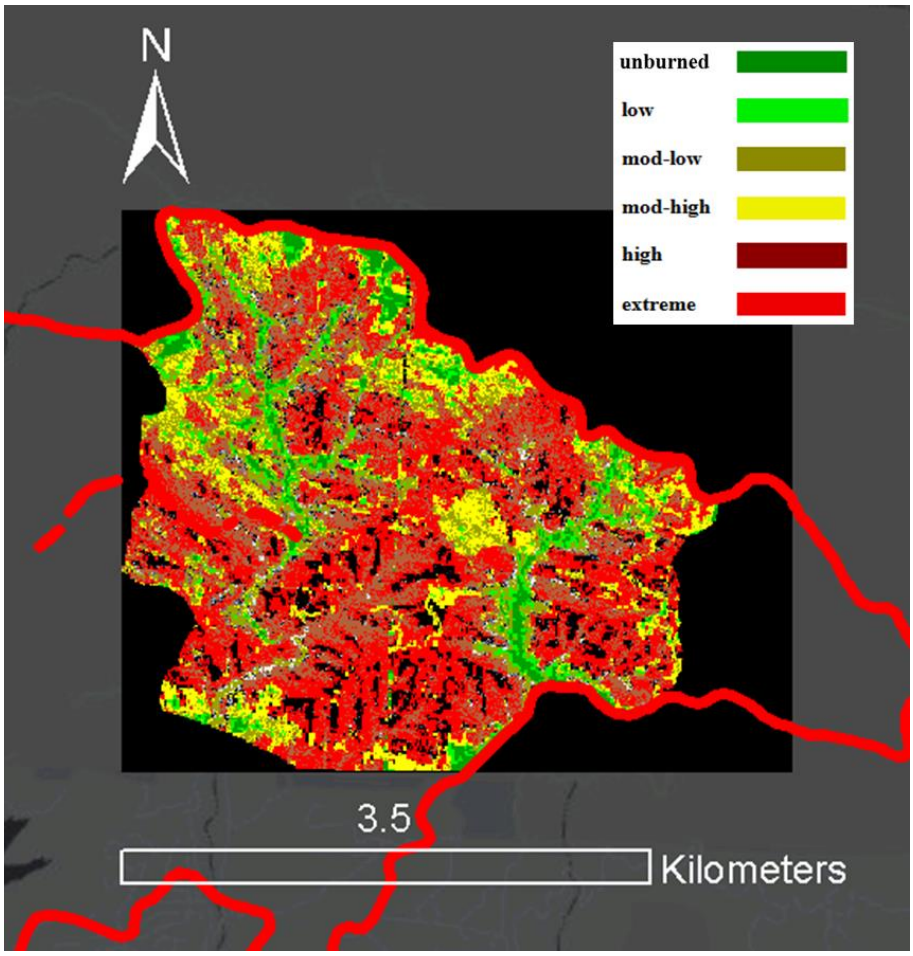

Figure IV-4: Jesusita fire map with the dNBR-MESMA-CHM based severity definition.

B. Topography and Fire Severity

Topographic factors are related to fire severity and vegetation structure survival, as shown in the CHM model derived from LiDAR (Figure IV-5). More biomass survived at the bottom of the valley or riparian area after the fire. In order to analyze the riparian-zone effect, a 50-meter radius buffer zone was developed along the river line (Figure IV-6).

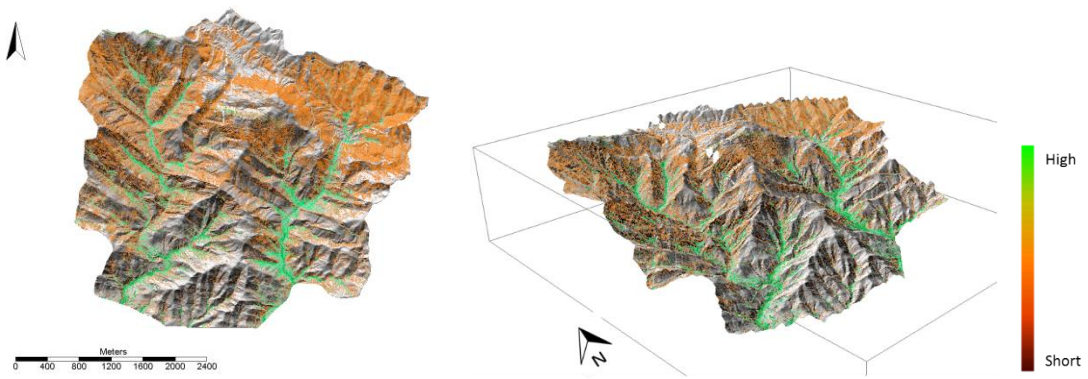

Figure IV-5: CHM model overlaid on DEM, with an orthophoto view (left) and 3D view (right).

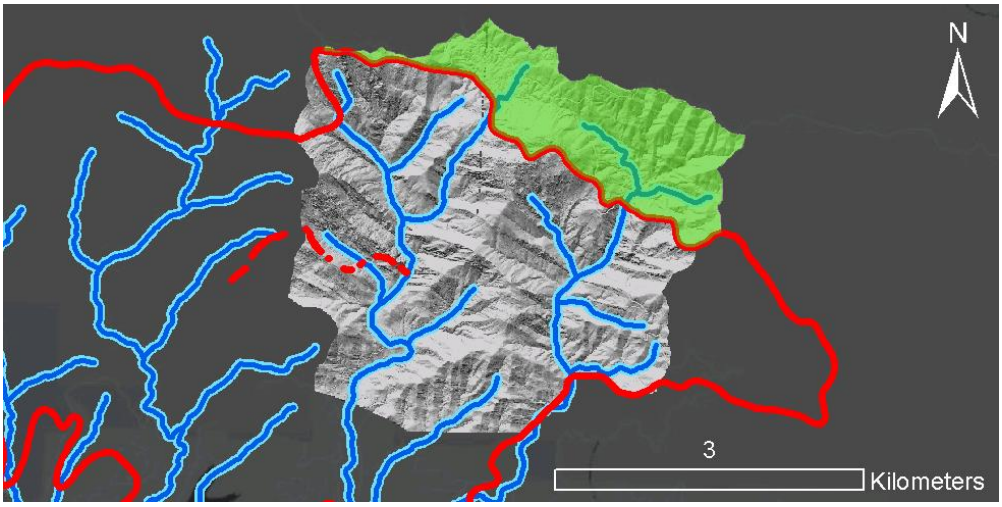

Figure IV-6: 50-meter radius riparian zone (light blue) derived from rivers (dark blue). The area outside Jesusita fire scar is overlaid with light green.

The distribution of the CHM in different dNBR level in the fire scar riparian zone shows large differences from the fire scar overall average (Figure IV-1), with a higher proportion of the vegetation structure over 10 meters in the unburned category. Outside of the fire scar, there is only a small difference between the riparian zone and overall average.

Applying a similar analysis using TWI (Figure III-6), a similar result was found (Figure IV-7). In the fire scar, more of the GV dominated area is preserved in the landscape with

TWI higher than 10, compared to the area outside the fire scar. If the TWI = 10 threshold is applied to the whole area, it is noticeable that a different level of TWI does produce large differences in the landscape, in terms of MESMA fraction percentage and CHM after the fire (Table IV-5). The largest differences come in Ash (0.399) and CHM (5.443m). For comparison, not much of a difference is shown in the area outside of the fire scar with different TWI levels. The mean and RSD of TWI tends to decrease as severity increases from unburned to the extreme level (Table IV-6), with an exception in the high level. This results from the CHM > 0 criteria in this level (Table IV-4), since many of the dead trunks standing after the fire come from the comparatively high TWI area.

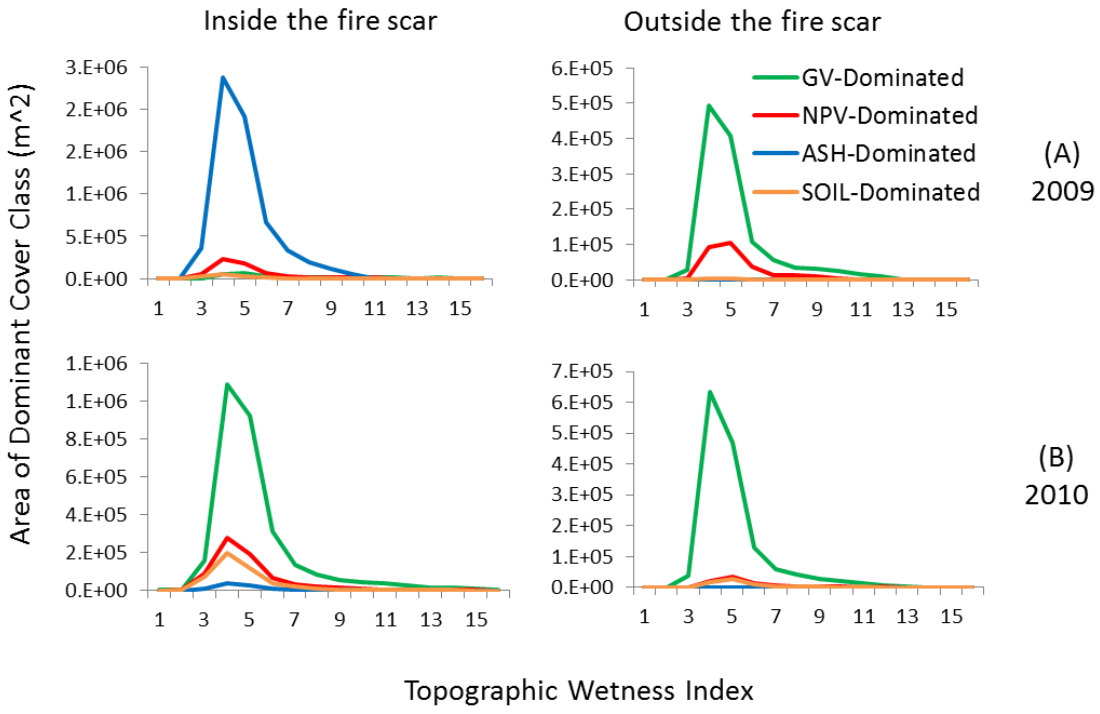

Figure IV-7: Different TWI and its corresponding MESMA domination type within LiDAR covered places in both 2009 (A) and 2010 (B).

Table IV-5: Average values of various data both inside and outside the fire scar, with and without the TWI>10 threshold.

Data	Inside Fire Scar		Outside Fire Scar	
	Overall average	TWI>10 average	Overall average	TWI>10 average
Ash	0.683	0.284	0.030	0.032
GV	0.070	0.334	0.599	0.577
NPV	0.127	0.296	0.309	0.272
Soil	0.031	0.013	0.044	0.068
dNBR	0.803	0.525	0.115	0.076
CHM(m)	2.493	7.936	2.293	4.688

Table IV-6: Mean, standard deviation and relative standard deviation for TWI in different fire severity levels inside the LiDAR fire scar.

	fire severity level	unburn	low	mod_low	mod_high	high	extreme
TWI	Mean	5.69	5.16	4.73	4.41	4.58	4.41
	SD	2.95	2.55	2.18	1.45	1.66	1.24
	RSD	0.52	0.49	0.46	0.33	0.36	0.28

C. Post-fire Recovery

Based on the dominant MESMA fraction type and CHM value in 2010 (Figure IV-2, B and D), green vegetation was increasing and short GV was balancing out the percentage of high GV compared to 2009 (Figure IV-2, A and C). The trend of regrowth is also clearly shown from a TWI perspective. There was significant amount of Ash dominated area with TWI value around 5 in 2009, but most of it turned into GV in 2010 (Figure IV-7). As a control group, there was no similar change pattern outside the fire scar.

A series of multi-temporal MESMA fraction images were derived from AVIRIS data (Figure IV-8) with fraction area percentage displayed in a timeline (Figure IV-9). Note that phenology could affect the recovery pattern since the images were acquired in different seasons. Major parts of the green vegetation did not recover until 04/2010, probably resulting

from the above average rainfall earlier that year. High levels of dead vegetation and soil in 2013 indicate that the 2012-2015 California droughts are slowing down the landscape from recovering to pre-fire conditions.

Note that there was some potential for human modification of post-fire recovery, e.g. the plane hydromulch applied in September 2009. The hydromulch is made up of recycled materials, and the goal is to stabilize the land and prevent erosion (Wohlgemuth, Beyers, & Robichaud, 2011). However, the covered area was only a small portion of the fire scar, and it did not overlap with the LiDAR covered (Figure IV-10).

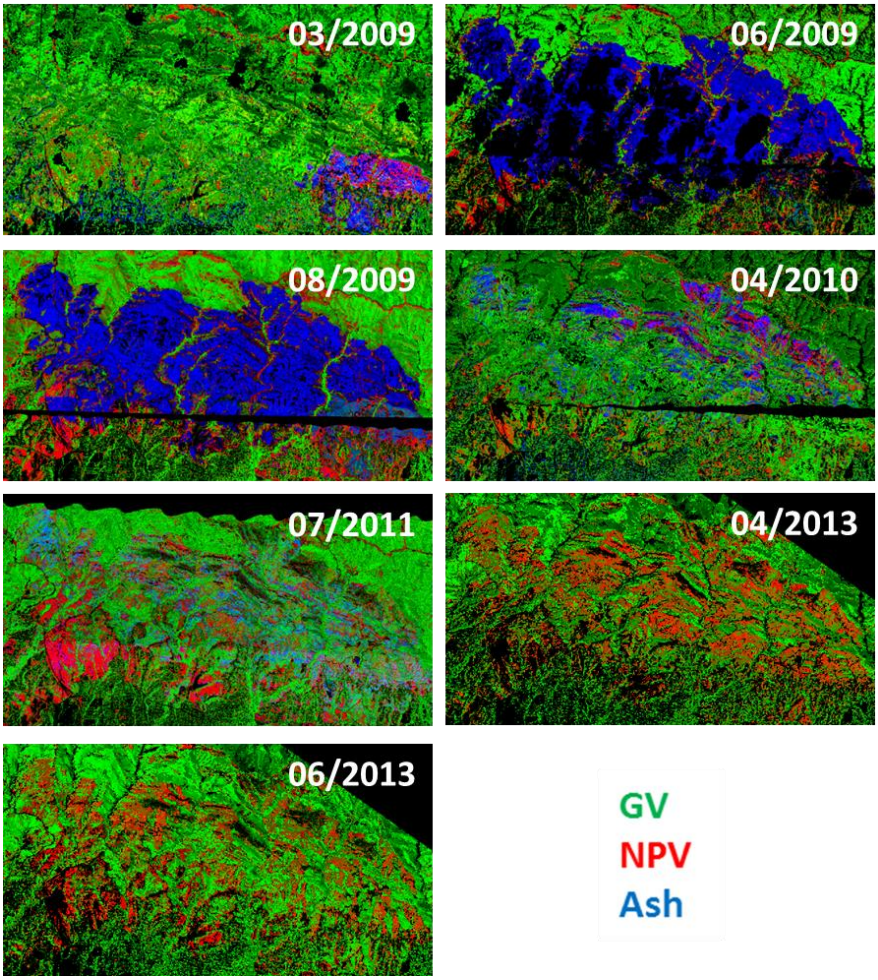

Figure IV-8: MESMA fraction map on multiple dates before and after the Jesusita fire. Significant parts of the 06/2009 image is unclassified due to smoke from the active fire.

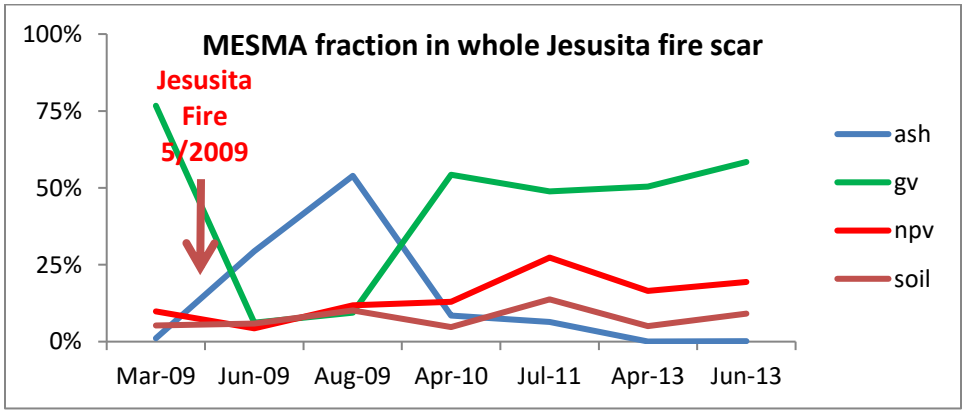

Figure IV-9: MESMA fraction map on multiple dates in the whole fire scar area.

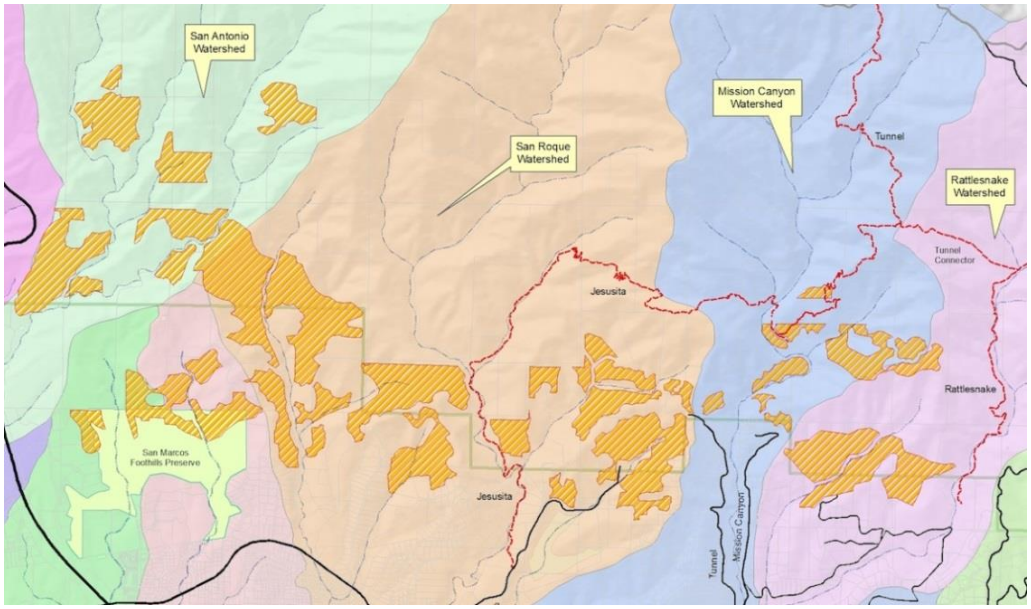

Figure IV-10: This map[2] shows areas in orange that were covered with hydromulch. The mulch was only applied to slopes between 30-60 percent, which is a small portion of the fire scar. Minor overlap occurs with the LiDAR covered area.

In order to examine topographic effects on post-fire recovery, the area covered by LiDAR was analyzed (Figure IV-11.A), which shows a similar trend compared to the whole fire scar (Figure IV-9). The area outside of fire scar acts as a control group, which reveals the phenology effect, e.g. a boost of NPV amount in August 2009 (Figure IV-11.C). GV fraction also varies among seasons, with a peak in June or July right before the summer drought (Table IV-7). GV fraction in the same season also varies among different years, resulting from different amounts of precipitation (Table IV-8). Inside the fire scar, the area with a TWI greater than 10 was less affected by the fire event (Figure IV-11.B) and returned to the pre-fire level at a faster rate. In July 2011, the TWI $\geq$ 10 areas inside the scar already reached

[2] Map created by Ray Ford (http://www.independent.com/news/2009/aug/27/county-unveils-hydromulch-program-jesusita-burn-ar/).

over 64.9% percent GV cover, while the whole scar average was 52.2%. As a result, TWI does affect recovery rate.

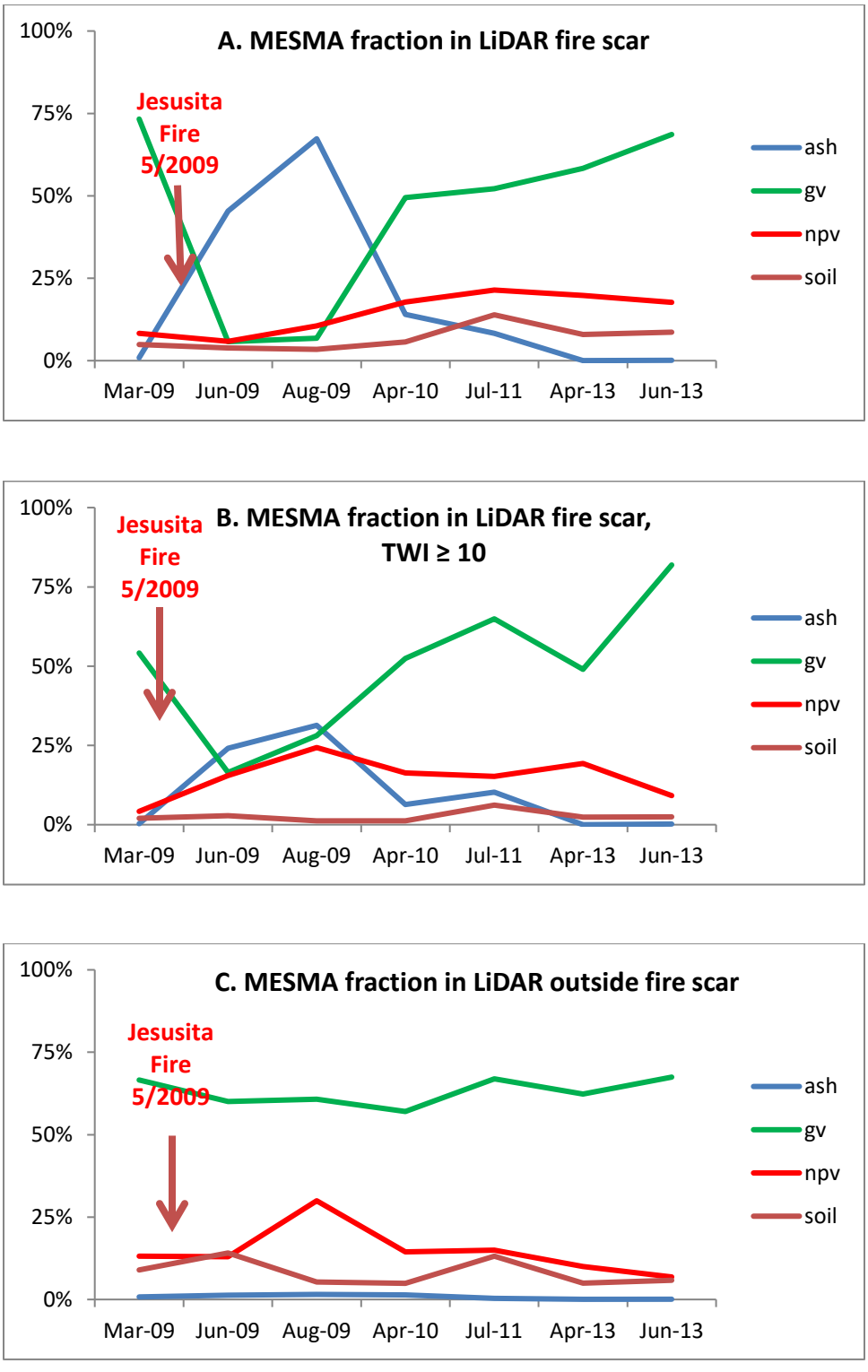

Figure IV-11: MESMA fraction map on multiple dates in the LiDAR area, including inside the fire scar (A), inside fire scar with TWI ≥ 10 (B) and outside fire scar (C). The sum of all MESMA fractions in June 2009 is low due to a significant amount of smoke and cloud in the scene, which results in large unclassified areas.

Table IV-7: Ash and GV fraction of different area, in multiple years. Spring (March and April) data are highlighted for comparison.

	LiDAR covered area	Pre-fire Mar-09	Post-fire Aug-09	Apr-10	Jul-11	Apr-13	Jun-13
Ash fraction	Inside scar	0.9%	67.3%	14.0%	8.3%	0.0%	0.1%
	Inside scar, TWI ≥ 10	0.3%	31.3%	6.4%	10.2%	0.0%	0.2%
	Outside scar	0.8%	1.5%	1.3%	0.4%	0.1%	0.1%
GV fraction	Inside scar	73.3%	6.8%	49.5%	52.2%	58.4%	68.7%
	Inside scar, TWI ≥ 10	54.2%	28.1%	52.5%	64.9%	49.0%	81.9%
	Outside scar	66.5%	60.8%	57.0%	67.0%	62.3%	67.5%

Table IV-8: Precipitation and fog data between different AVIRIS acquisition dates, recorded from Coal Oil Point Reserve (http://www.geog.ucsb.edu/ideas/).

	Duration sum (mm)		Daily average (mm)	
	rain	fog	rain	Fog
Aug-09				
	473.9	25.6	0.0199	0.00108
Apr-10				
	664.2	59.1	0.0155	0.00138
Jul-11				
	507.2	50.2	0.00834	0.00083
Apr-13				
	1.778	2.4	0.00032	0.00043
Jun-13				

Conclusion

By combining airborne hyperspectral and LiDAR remote sensing data, the 2009 Jesusita Fire event can be clearly detected. The MESMA fraction map together with CHM and DEM provide more nuanced and detailed analysis of the fire severity and post-fire recovery.

The dNBR-MESMA-CHM based fire severity provided a better insight into fire severity compared to the traditional dNBR metric. dNBR is only able to provide the cover change during the fire, while not revealing the actual land-cover fractions and vertical structure after the event. More than 60% of the fire scar ended up in high biomass lost or ash dominated category, while half of area retained some dead trunks. The LiDAR metric is necessary to separate half of the original “high severity” areas into the new “extreme severity” areas.

The riparian zone and the areas with high surface soil moisture protected the biomass from fire. For image pixels with TWI larger than 10, the GV fraction average was 0.334 comparing to the whole fire scar average 0.070. The average of CHM was also higher, increasing from 2.493m to 7.936m. During the post-fire recovery process, the GV and ash fraction in those areas also returned to the pre-fire level at a faster rate compared to the drier landscape.

There are limitations of this research, as a pixel based CHM map can produce more error when the canopy is spread across several pixels. This could potentially be solved by separating individual vegetation crowns from LiDAR point clouds and analyzing biomass on an object basis. However, a fieldwork measuring detailed ground vegetation metrics would be demanded to verify such delicate algorithms. In addition, it would have been highly

beneficial to have pre-fire LiDAR, to evaluate height change following fire. Some high severity areas with low CHM may have had low CHM prior to the fire.

References

Adams, J. B., Sabol, D. E., Kapos, V., Almeida Filho, R., Roberts, D. A., Smith, M. O., & Gillespie, A. R. (1995). Classification of multispectral images based on fractions of endmembers: Application to land-cover change in the Brazilian Amazon. *Remote Sensing of Environment*, *52*(2), 137–154. http://doi.org/10.1016/0034-4257(94)00098-8

Bastos, A., Gouveia, C. M., Dacamara, C. C., & Trigo, R. M. (2011). Modelling post-fire vegetation recovery in Portugal. *Biogeosciences*, *8*(12), 3593–3607. http://doi.org/10.5194/bg-8-3593-2011

Beven, K. J., & Kirkby, M. J. (1979). A physically based, variable contributing area model of basin hydrology. *Hydrological Sciences Journal*, *24*(1), 43–69. http://doi.org/10.1080/02626667909491834

Brown, J. K., & Smith., J. K. (2000). Wildland fire in ecosystems: effects of fire on flora. *Gen. Tech. Rep. RMRS-GTR-42*, *2*, 257. http://doi.org/10.1111/j.1467-7717.2009.01106.x

Casas, Á., García, M., Siegel, R. B., Koltunov, A., Ramírez, C., & Ustin, S. (2016). Burned forest characterization at single-tree level with airborne laser scanning for assessing wildlife habitat. *Remote Sensing of Environment*, *175*, 231–241. http://doi.org/10.1016/j.rse.2015.12.044

Chen, X., Vogelmann, J. E., Rollins, M., Ohlen, D., Key, C. H., Yang, L., … Shi, H. (2011). Detecting post-fire burn severity and vegetation recovery using multitemporal remote sensing spectral indices and field-collected composite burn index data in a ponderosa

pine forest. *International Journal of Remote Sensing*, *32*(23), 7905–7927. http://doi.org/10.1080/01431161.2010.524678

Chirico, G. B., Western, A. W., & Grayson, R. B. (2005). On the definition of the flow width for calculating specific catchment area patterns from gridded elevation data. *Hydrological Processes*, *19*(13), 2539–2556. http://doi.org/10.1002/hyp.5730

Chu, T., & Guo, X. (2014). Remote sensing techniques in monitoring post-fire effects and patterns of forest recovery in boreal forest regions: A review. *Remote Sensing*, *6*(1), 470–520. http://doi.org/10.3390/rs6010470

Chuvieco, E. (Ed. . (2009). *Earth Observation of Wildland Fires in Mediterranean Ecosystems*. *Dordrecht, The Netherlands: Springer*. http://doi.org/10.1017/CBO9781107415324.004

Clark, R. N., Swayze, G. A., Livo, K. E., Kokaly, R. F., King, T. V. V. ., Dalton, J. B., … Mcdougal, R. R. (2002). Surface Reflectance Calibration of Terrestrial Imaging Spectroscopy Data: a Tutorial Using AVIRIS. *Proceedings of the 10th AirborneEarth Science Workshop*, 1–21.

Davis, F. W., & Michaelsen, J. (1995). Sensitivity of fire regime in chaparral ecosystems to climate change. *Global Change and Mediterranean-Type Ecosystems*, 435–456.

Dennison, P. E., Halligan, K. Q., & Roberts, D. A. (2004). A comparison of error metrics and constraints for multiple endmember spectral mixture analysis and spectral angle mapper, *93*, 359–367. http://doi.org/10.1016/j.rse.2004.07.013

Dennison, P. E., & Roberts, D. A. (2003a). Endmember selection for multiple endmember

spectral mixture analysis using endmember average RMSE, *87*, 123–135. http://doi.org/10.1016/S0034-4257(03)00135-4

Dennison, P. E., & Roberts, D. A. (2003b). The effects of vegetation phenology on endmember selection and species mapping in southern California chaparral. *Remote Sensing of Environment*, *87*(2–3), 295–309. http://doi.org/10.1016/j.rse.2003.07.001

Escuin, S., Navarro, R., & Fernández, P. (2008). Fire severity assessment by using NBR (Normalized Burn Ratio) and NDVI (Normalized Difference Vegetation Index) derived from LANDSAT TM/ETM images. *International Journal of Remote Sensing*, *29*(4), 1053–1073. http://doi.org/10.1080/01431160701281072

French, N., Kasischke, E., Hall, R., Murphy, K., Verbyla, D., Hoy, E., & Allen, J. (2008). Using Landsat data to assess fire and burn severity in the North American boreal forest region: an overview and summary of results. *International Journal of Wildland Fire*, *17*(4), 443–462. http://doi.org/10.1071/WF08007

García, M. J. L., & Caselles, V. (1991). Mapping burns and natural reforestation using thematic Mapper data. *Geocarto International*, *6*(1), 31–37. http://doi.org/10.1080/10106049109354290

Green, R. O., Eastwood, M. L., Sarture, C. M., Chrien, T. G., Aronsson, M., Chippendale, B. J., … Williams, O. (1998). Imaging spectroscopy and the Airborne Visible/Infrared Imaging Spectrometer (AVIRIS). *Remote Sensing of Environment*, *65*(3), 227–248. http://doi.org/10.1016/S0034-4257(98)00064-9

Hanes, T. L. (1977). California Chaparral. In M. G. Barbour & J. Major (Eds.), *Terrestrial*

vegetation of California (pp. 417–469). John Wiley and Sons.

Harrison, A. T., Small, E., & Mooney, H. A. (1971). Drought Relationships and Distribution of Two Mediterranean-Climate California Plant Communities. *Ecology*, *52*(5), 869–875.

Hyde, P., Dubayah, R., Walker, W., Blair, J. B., Hofton, M., & Hunsaker, C. (2006). Mapping forest structure for wildlife habitat analysis using multi-sensor (LiDAR, SAR/InSAR, ETM+, Quickbird) synergy. *Remote Sensing of Environment*, *102*(1–2), 63–73. http://doi.org/10.1016/j.rse.2006.01.021

Kane, V. R., McGaughey, R. J., Bakker, J. D., Gersonde, R. F., Lutz, J. a., & Franklin, J. F. (2010). Comparisons between field- and LiDAR-based measures of stand structural complexity. *Canadian Journal of Forest Research*, *40*(4), 761–773. http://doi.org/10.1139/X10-024

Keddy, P. (2007). *Plants and vegetation: origins, processes, consequences*. Cambridge University Press.

Keeley, J. E. (2009). Fire intensity, fire severity and burn severity: a brief review and suggested usage. *International Journal of Wildland Fire*, *18*(1), 116. http://doi.org/10.1071/WF07049

Kokaly, R. F., Rockwell, B. W., Haire, S. L., & King, T. V. V. (2007). Characterization of post-fire surface cover, soils, and burn severity at the Cerro Grande Fire, New Mexico, using hyperspectral and multispectral remote sensing. *Remote Sensing of Environment*, *106*(3), 305–325. http://doi.org/10.1016/j.rse.2006.08.006

Lefsky, M. a., Cohen, W. B., Parker, G. G., & Harding, D. J. (2002). Lidar Remote Sensing

for Ecosystem Studies. *BioScience*, *52*(1), 19. Retrieved from http://www.jstor.org/stable/10.1641/0006-3568(2002)052[0019:LRSFES]2.0.CO;2

Lefsky, M. A., Turner, D. P., Guzy, M., & Cohen, W. B. (2005). Combining lidar estimates of aboveground biomass and Landsat estimates of stand age for spatially extensive validation of modeled forest productivity. *Remote Sensing of Environment*, *95*(4), 549–558. http://doi.org/10.1016/j.rse.2004.12.022

Lentile, L. B., Holden, Z. A., Smith, A. M. S., Falkowski, M. J., & Hudak, A. T. (2006). Remote sensing techniques to assess active fire characteristics and post fire effects. *USDA Forest Service / UNL Faculty Publications*, *194*(15), 319–345.

Lutes, D. C., Keane, R. E., Caratti, J. F., Key, C. H., Benson, N. C., Sutherland, S., & Gangi, L. J. (2007). *FIRMON: Fire Effects Monitoring and Inventory System*. Rocky Mountain Research Station.

Miller, J. D., & Thode, A. E. (2007). Quantifying burn severity in a heterogeneous landscape with a relative version of the delta Normalized Burn Ratio (dNBR). *Remote Sensing of Environment*, *109*(1), 66–80. http://doi.org/10.1016/j.rse.2006.12.006

Miller, J. D., & Yool, S. R. (2002). Mapping forest post-fire canopy consumption in several overstory types using multi-temporal Landsat TM and ETM data. *Remote Sensing of Environment*, *82*(2–3), 481–496. http://doi.org/10.1016/S0034-4257(02)00071-8

Moore, I. D., Burch, G. J., & Mackenzie, D. H. (1988). Topographic Effects on the Distribution of Surface Soil Water and the Location of Ephemeral Gullies. *Transactions of the ASAE*, *31*(4), 1098–1107. Retrieved from

http://asae.frymulti.com/abstract.asp?adid=30829&t=3

Moore, I. D., Grayson, R. B., & Ladson, a R. (1991). Digital Terrain Modeling : A Review of Hydrological Geomorphological and Biological Applications. *Hydrological Processes*, *5*(1), 3–30. http://doi.org/DOI: 10.1002/hyp.3360050103

Moreno, J. M., & Oechel, W. C. (1991). Fire Intensity Effects on Germination of Shrubs and Herbs in Southern California Chaparral. *Ecology*, *72*(6), 1993–2004.

Quintano, C., Fernández-Manso, A., & Roberts, D. A. (2013). Multiple Endmember Spectral Mixture Analysis (MESMA) to map burn severity levels from Landsat images in Mediterranean countries. *Remote Sensing of Environment*, *136*, 76–88. http://doi.org/10.1016/j.rse.2013.04.017

Riano, D., Chuvieco, E., Ustin, S., Zomer, R., Dennison, P., Roberts, D., & Salas, J. (2002). Assessment of vegetation regeneration after fire through multitemporal analysis of AVIRIS images in the Santa Monica Mountains. *Remote Sensing of Environment*, *79*(1), 60–71. http://doi.org/10.1016/S0034-4257(01)00239-5

Roberts, D. A., Bradley, E., Roth, K. L., Eckmann, T., & Still, C. J. (2010). Linking Physical Geography Education and Research Through the Development of an Environmental Sensing Network and Project- Based Learning. *Journal of Geoscience Education*, *58*(5), 262–274.

Roberts, D. A., Dennison, P. E., Gardner, M. E., Hetzel, Y., Ustin, S. L., & Lee, C. T. (2003). Evaluation of the potential of Hyperion for fire danger assessment by comparison to the airborne visible/infrared imaging spectrometer. *IEEE Transactions on Geoscience and*

Remote Sensing, *41*(6 PART I), 1297–1310. http://doi.org/10.1109/TGRS.2003.812904

Roberts, D. A., Dennison, P. E., Roth, K. L., Dudley, K., & Hulley, G. (2015). Relationships between dominant plant species, fractional cover and Land Surface Temperature in a Mediterranean ecosystem. *Remote Sensing of Environment*, *167*(February), 152–167. http://doi.org/10.1016/j.rse.2015.01.026

Roberts, D. A., Gardner, M., Church, R., Ustin, S., Scheer, G., & Green, R. O. (1998). Mapping chaparral in the Santa Monica Mountains using multiple endmember spectral mixture models. *Remote Sensing of Environment*, *65*(3), 267–279. http://doi.org/10.1016/S0034-4257(98)00037-6

Roberts, D. A., Green, R. O., & Adams, J. B. (1997). Temporal and spatial patterns in vegetation and atmospheric properties from AVIRIS. *Remote Sensing of Environment*, *62*(3), 223–240. http://doi.org/10.1016/S0034-4257(97)00092-8

Roberts, D. a., Quattrochi, D. a., Hulley, G. C., Hook, S. J., & Green, R. O. (2012). Synergies between VSWIR and TIR data for the urban environment: An evaluation of the potential for the Hyperspectral Infrared Imager (HyspIRI) Decadal Survey mission. *Remote Sensing of Environment*, *117*, 83–101. http://doi.org/10.1016/j.rse.2011.07.021

Roberts, D. A., Smith, M. O., & Adams, J. B. (1993). Green, Vegetation, Nonphotosynthetic Vegetation, and Soil in AVIRIS Data, 255–269.

Roberts, D., Halligan, K., & Dennison, P. (2007). *VIPER Tools User Manual*.

Röder, A., Hill, J., Duguy, B., Alloza, J. A., & Vallejo, R. (2008). Using long time series of Landsat data to monitor fire events and post-fire dynamics and identify driving factors.

A case study in the Ayora region (eastern Spain). *Remote Sensing of Environment*, *112*(1), 259–273. http://doi.org/10.1016/j.rse.2007.05.001

Sankey, T. T., Moffet, C. A., & Weber, K. (2008). Postfire Recovery of Sagebrush Communities : Assessment Using SPOT-5 and Very Large-Scale Aerial Imagery. *Rangeland Ecology and Management*, *61*(6), 598–604. http://doi.org/10.2111/08-079.1

Schimmel, J., & Granstrom, A. (1996). Fire severity and vegetation response in the boreal Swedish forest. *Ecology*, *77*(5), 1436–1450.

Smith, A. M. S., Lentile, L. B., Hudak, A. T., & Morgan, P. (2007). Evaluation of linear spectral unmixing and ΔNBR for predicting post-fire recovery in a North American ponderosa pine forest. *International Journal of Remote Sensing*, *28*(22), 5159–5166. http://doi.org/10.1080/01431160701395161

Souza, C., Firestone, L., Silva, L. M., & Roberts, D. (2003). Mapping forest degradation in the Eastern Amazon from SPOT 4 through spectral mixture models. *Remote Sensing of Environment*, *87*(4), 494–506. http://doi.org/10.1016/j.rse.2002.08.002

Tompkins, S., Mustard, J. F., Pieters, C. M., & Forsyth, D. W. (1997). Optimization of endmembers for spectral mixture analysis. *Remote Sensing of Environment*, *59*(3), 472–489. http://doi.org/10.1016/S0034-4257(96)00122-8

van Wagtendonk, J. W., Root, R. R., & Key, C. H. (2004). Comparison of AVIRIS and Landsat ETM+ detection capabilities for burn severity. *Remote Sensing of Environment*, *92*(3), 397–408. http://doi.org/10.1016/j.rse.2003.12.015

Veraverbeke, S., Lhermitte, S., Verstraeten, W., & Goossens, R. (2011). A time-integrated

MODIS burn severity assessment using the multi-temporal differenced normalized burn ratio (dNBRMT). *International Journal of Applied Earth Observation and Geoinformation*, *13*(1), 52–58. http://doi.org/10.1016/j.jag.2010.06.006

Veraverbeke, S., Lhermitte, S., Verstraeten, W. W., & Goossens, R. (2010). The temporal dimension of differenced Normalized Burn Ratio (dNBR) fire/burn severity studies: The case of the large 2007 Peloponnese wildfires in Greece. *Remote Sensing of Environment*, *114*(11), 2548–2563.

Veraverbeke, S., Somers, B., Gitas, I., Katagis, T., Polychronaki, A., & Goossens, R. (2012). Spectral mixture analysis to assess post-fire vegetation regeneration using Landsat Thematic Mapper imagery: accounting for soil brightness variation. *International Journal of Applied Earth Observation and Geoinformation*, *14*(1), 1–11.

Vila, J. P. S., & Barbosa, P. (2010). Post-fire vegetation regrowth detection in the Deiva Marina region (Liguria-Italy) using Landsat TM and ETM+ data. *Ecological Modelling*, *221*(1), 75–84. http://doi.org/10.1016/j.ecolmodel.2009.03.011

Western, A. W., Grayson, R. B., Bschl, G., & Willgoose, G. R. (1999). Observed spatial organization of soil moisture indices. *Water Resources Research*, *35*(3), 797–810.

White, D., Minotti, P. G., Barczak, M. J., Sifneos, J. C., Kathryn, E., Santelmann, M. V, … Preston, E. M. (1997). Society for Conservation Biology Assessing Risks to Biodiversity from Future Landscape Change Linked references are available on JSTOR for this article : Assessing Risks to Biodiversity from Future Landscape Change. *Conserv. Biol.*, *11*(2), 349–360.

White, J. D., Ryan, K. C., Key, C. C., & Running, S. W. (1996). Remote Sensing of Forest Fire Severity and Vegetation Recovery. *International Journal of Wildland Fire*, *6*(3), 125. http://doi.org/10.1071/WF9960125

Wohlgemuth, P. M., Beyers, J. L., & Robichaud, P. R. (2011). The Effectiveness of Aerial Hydromulch as an Erosion Control Treatment in Burned Chaparral Watersheds , Southern California. In *The Fourth Interagency Conference on Research in the Watersheds* (pp. 26–30).

Zaslavsky, D. (1981). Surface Hydrology: I—Explanation of Phenomena. *Journal of the Hydraulics Division*, *107*(1), 1–16.